Effects of Wind-Powered Hydrogen Fuel Cell Vehicles on Stratospheric Ozone and Global Climate

Mark Z. Jacobson

Department of Civil and Environmental Engineering, Stanford University, Stanford, California 94305-4020, USA; Email: jacobson@stanford.edu; Tel: (650) 723-6836

Supplementary Material

S1. Introduction.

This document describes the model and emission scenarios used for this study. The emission scenarios include a baseline emission scenario and a wind-powered hydrogen-fuel cell vehicle emission scenario. The document also develops a method of converting pseudo-first-order rate coefficients of heterogeneous chemical reactions to second-order rate coefficients to ensure mass conservation. Finally, the document provides figures used in the main text and calculates the number of wind turbines and land use required for wind-powered hydrogen fuel cell vehicles and wind-powered battery electric vehicles.

S2. Model. The model used was GATOR-GCMOM, which solves dynamical, gas, aerosol, cloud, transport, radiation, and surface processes [*Jacobson*, 2001-2006]. The model has been tested against meteorological, chemical, and radiative field data without nesting on urban scales [*Jacobson*, 1997], with nesting from the global-through-urban scale [*Jacobson*, 2001b], with nesting from the global-through-regional scale [*Jacobson et al*., 2004, 2005; 2006, 2007], and on the global scale [*Jacobson*, 2001c, 2002b; 2004]. Simulations were run on a 4° S-N x 5° W-E global domain with 47 layers up to 0.22 hPa (≈60 km), including 6 from 0-1 km, 24 from 1-15 km, and 17 from 15-60 km.

Gas photochemistry was solved among 128 gases and 391 reactions [314 kinetic reactions (33 chlorine and 18 bromine), 20 heterogeneous reactions (9 on each aerosol particles and frozen hydrometeor particles and 2 on liquid hydrometeor surfaces), and 57 photolysis reactions (including 13 chlorine and 8 bromine) with SMVGEAR II [*Jacobson*, 1998]. Reactions and kinetic rate coefficients are given in the Reaction List at the end of this document.

Aerosol processes included size- and composition-resolved emissions, sulfuric acid binary and ternary homogeneous nucleation (solved together with sulfuric acid condensation), secondary organic gas condensation, aerosol-aerosol coagulation, cloud activation, aerosol-cloud coagulation, nonequilibrium dissolution of NH_3, HNO_3, HCl coupled with internal aerosol solution-phase and solution-solid equilibrium chemistry, and sedimentation [*Jacobson*, 2002a, 2003, 2005a].

Aerosols were treated over two discrete size distributions, each with 14 size bins (0.002 to 50 μm in diameter), and three hydrometeor distributions, each with 30 bins (Table S1). Particle number concentration and mole concentrations of several chemicals were predicted in each aerosol and hydrometeor size bin of each distribution. The aerosol distributions were an emitted fossil-fuel soot (EFFS) and an internally-mixed (IM) distribution. BC, POM, H_2SO_4(aq), HSO_4^-, and SO_4^{2-} were emitted into each bin of the EFFS distribution. Other species [H_2O, SOM, NO_3^-, Cl^-, H^+, NH_4^+, NH_4NO_3(s), $(NH_4)_2SO_4$(s)] formed in the distribution by gas-to-particle conversion or crystallization. The IM distribution consisted of the chemicals in the EFFS distribution plus Na^+, soil dust, pollen, spores, and bacteria. All emissions aside from fossil-fuel soot, entered the IM distribution. Emitted sea spray included H_2O, Na^+, K^+, Mg^{2+}, Ca^{2+}, Cl^-, NO_3^-, H_2SO_4(aq), HSO_4^-, and SO_4^{2-}. Biomass and biofuel burning included the same aerosol species plus BC and POM. In both cases, K^+, Mg^{2+}, and Ca^{2+} were treated as equivalent Na^+. Other emissions included pollen/spores/bacteria (treated as one species) and soildust.

The two aerosol distributions evolved into three discrete, size-resolved hydrometeor distributions: liquid, ice, and graupel, each of which contained the underlying aerosol components they formed on (Table S1). The thermodynamics and microphysics of the convective subgrid and stratus grid-scale cloud treatments is given in *Jacobson* [2003]. Briefly, cloud microphysical processes included condensation/evaporation, deposition, sublimation, liquid-liquid, liquid-ice, liquid-graupel, ice-ice, ice-graupel, graupel-graupel coagulation, liquid-aerosol, ice-aerosol, and graupel-aerosol coagulation, liquid drop breakup, contact freezing (resulting from liquid-aerosol coagulation at subfreezing temperatures), homogeneous/heterogeneous freezing, evaporative freezing, melting, lightning formation due to charge separation from size-resolved bounceoffs, and sedimentation. Precipitation drops contained the aerosol constituents it grew upon. Cloud-aerosol interactions have been evaluated in *Jacobson* [2003] and *Jacobson et al*. [2006, 2007].

To calculate condensation/evaporation and deposition/sublimation, the total number concentration of aerosol particles in each size bin of each aerosol distribution was divided into ice deposition nuclei (IDN), cloud condensation nuclei (CCN), and other, as described in *Jacobson* [2003]. The fractions were based on current aerosol composition in the bin. Nonequilibrium condensation and deposition equations were then solved simultaneously among the gas phase and CCN and IDN in all size bins of both aerosol distributions. Thus, when supercooled clouds formed, deposition competed with condensation for the limited amount of vapor available. Because aerosol particles were transported vertically with cloud water within all subgrid scale convective clouds, aerosol activation was consistent with that in a rising plume.

Activated CCN and IDN and the water grown on them were partitioned into separate liquid and ice hydrometeor size distributions. For example, each size bin of the liquid hydrometeor distribution contained some particles and their chemical components activated from the EFFS aerosol distribution and others from the IM distribution.

Unactivated CCN and IDN in each aerosol distribution stayed as interstitial aerosols. A third discretized hydrometeor distribution, graupel, was also tracked. The graupel distribution formed upon heterocoagulation of liquid water and ice hydrometeor distributions, contact freezing of aerosol particles with the liquid distribution, heterogeneous-homogeneous freezing of the liquid distribution, and evaporative freezing of the liquid distribution. Graupel also contained aerosol inclusions. Thus, within each size bin of each hydrometeor type, all aerosol components that the hydrometeor grew on (listed in Table S1) were tracked. Interstitial size-resolved aerosol particles within clouds also coagulated with hydrometeor particles of different size, and these aerosol chemicals were tracked within the hydrometeor particles as well.

Heterogeneous reactions in the stratosphere can occur on several types of particles, including sulfuric acid tetrahydrate (SAT), sulfuric acid hemihexahydrate (SAH), supercooled ternary solutions (STS), nitric acid trihydrate (NAT), nitric acid dihydrate (NAD), and water-ice, among others [e.g., *Toon et al*., 1986; *Hanson and Mauersberger*, 1988; *Turco et al*., 1989; *Worsnop et al*., 1993; *Zhang et al*., 1993; *Tabazadeh and Turco*, 1993; *Drdla et al*., 2002a,b,c; *Jensen et al*., 2002; *Strawa et al*., 2002; *Sander et al*., 2006]. In the troposphere, heterogeneous reactions also occur on liquid hydrometeor particles. In reality, pure forms of such particles are rare, as all contain at least trace amounts of other chemicals.

In the model, heterogeneous aerosol reactions occurred on the two aerosol distributions. Heterogeneous water-ice and NAT reactions occurred on both the ice and graupel hydrometeor distributions (where the determination of whether the ice and graupel distributions were covered with water ice or NAT is described shortly). Heterogeneous liquid reactions occurred on the liquid hydrometeor distribution.

Each size bin of each aerosol size distribution contained a different quantity of each chemical listed in Table S1, including nitrate, sulfate, and supercooled or warm liquid water, among others. Aerosol pH and liquid water content in each size bin of each

aerosol distribution in the stratosphere (and elsewhere) were determined from EQUISOLV II [*Jacobson*, 2005a], which treats solute activity coefficients of many chemicals at temperatures down to 190 K following the activity coefficient parameterization of *Lin and Tabazadeh* [2001]. Other processes affecting these aerosol particles included transport, binary (at low ammonia) and ternary homogeneous nucleation, coagulation, condensation (e.g., of sulfuric acid, organics), dissolution (e.g., of nitric acid, hydrochloric acid), and sedimentation. The composition of stratospheric aerosols varied with size and location. Some were primarily sulfate-water; others sulfate-ammonium-water, others nitrate-water, but all had trace amounts of all chemicals (e.g., down to machine precision).

Each size bin of each hydrometeor size distribution contained all the chemical components found in aerosol particles (Table S1). Chemicals entered hydrometeor particles primarily during nucleation scavenging and aerosol-hydrometeor coagulation. In addition, nitric acid grew by deposition onto the size-resolved ice and graupel hydrometeor distributions when (a) its partial pressure exceeded its saturation vapor pressure along ice/NAT boundaries and (b) the partial pressure of water was lower then its saturation vapor pressure along ice/NAT boundaries, as determined from equations in Table 1 of *Hanson and Mauersberger* [1988]. The solution scheme for nitric acid depositional growth was the Analytical Predictor of Condensation (APC) scheme, given in *Jacobson* [2002a]. If nitric acid deposited onto ice according to the conditions above, the surface was assumed to be converted to NAT.

Sulfur dioxide, hydrogen peroxide, and ozone also entered liquid cloud drops and oxidized irreversibly to S(VI) compounds (H_2SO_4(aq), HSO_4^-, and SO_4^{2-}). All other gases in the model also entered precipitation reversibly according to their Henry's law partitioning and were either carried to lower levels where they evaporated or were removed when precipitation reached the ground [*Jacobson*, 2003].

Heterogeneous reactions occurred on all aerosol and hydrometeor size distributions. The reaction list (end of document) shows that three reactions, $N_2O_5 + H_2O$, $ClONO_2 + H_2O$, and $BrONO_2 + H_2O$ occurred on liquid hydrometeor particle surfaces. Nine reactions occurred on aerosol and ice surfaces and five occurred on NAT surfaces. The products of heterogeneous reactions were dissolved or adsorbed nitric acid or water, and halogen gases. Since aerosol particles and hydrometeor particles were size-resolved and sank based on their individual fall speeds, sedimentation allowed explicit treatment of stratospheric denitrification. Upon evaporation or sublimation of the hydrometeor particles, nitric acid and other inclusions within hydrometeor particles were released back to the air as aerosol particles. Nitric acid could then evaporate from aerosol particles if conditions were right. If hydrometeor particles fell to the ground, they and their inclusions were treated as precipitation.

Reaction probabilities on NAT, water ice, liquid, and aerosol particles were obtained from the references listed in the reaction list. Most reaction probabilities were temperature and partial-pressure dependent [e.g., *Tabazadeh and Turco*, 1993; *Robinson et al.,* 1997; *Shi et al*., 2001]. Others were assumed to be independent of temperature. Because aerosol particles are present at all temperatures, reactions could always occur over the observed temperature ranges of the reaction probabilities.

Heterogeneous (gas-particle) chemistry was calculated together with homogeneous gas-phase kinetic and photochemistry with SMVGEAR II. The pseudo-first-order rate coefficient (s^{-1}) of a heterogeneous reaction, $E(g) \xrightarrow{\Gamma(a)} G(g)+H(a)$, where E is a gas and F is adsorbed to a particle surface, is generally written as

$$k_{r,E} = \frac{1}{4}\bar{v}_E \gamma_{E,F} a \qquad \text{(S1)}$$

where $\bar{v}_E$ is the thermal speed of gas E (cm/s), $\gamma_{E,F}$ is the reaction probability (dimensionless) of gas E with adsorbed gas F, and a is the surface-area concentration (e.g., square centimeters of surface per cubic centimeter of air) summed over all particles

of all sizes in all size distributions in which reactions occur. In the case of reactions on aerosol surfaces, it is the area concentration summed over the two aerosol distributions in Table S1. In the case of reactions on liquid cloud surfaces, it is the area concentration summed over the liquid hydrometeor distribution in Table S1. In the case of reactions on ice cloud surface, it is the area concentration summed over the ice and graupel hydrometeor distributions in Table S1. The thermal speed is calculated as $\bar{v}_E = \sqrt{8k_B TA/\pi m_E}$, where k_B is Boltzmann's constant, T is absolute temperature, A is Avogadro's number, and m_E is the molecular weight of species E.

Because Equation S1 implicitly includes the concentration of an adsorbed reactant but not of the gas reactant; it is a pseudo-first-order rate coefficient (s^{-1}). However, in order to conserve mass of all chemicals in the atmosphere, it is necessary to track the reduction in mass of the adsorbed reactant, whether it is H_2O, HCl, or HBr, in the reaction. To do this, it is necessary to convert Equation S1 to a second-order rate coefficient (cm^3 molec. s^{-1}). This can be done either by first calculating the transfer of gas F to particle surfaces and then solving for the change in F as an adsorbed species in a second-order reaction with E or by solving for F as a gas in a second-order reaction with E, but including the estimated transfer of F to surfaces in the rate coefficient. The latter method was chosen here since it is requires significantly less computational resources. The resulting second-order reaction is $E(g) + F(g) \rightarrow G(g) + H(a)$, where the second-order rate coefficient (cm^3 molec.$^{-1}$ s^{-1}) is now determined as

$$k_{s,E,F} = \frac{1}{4} \frac{\bar{v}_E \gamma_{E,F}}{n_m} \frac{N_{s,F,\mathrm{int}}}{N_{g,F,s-h}} \qquad \text{(S2)}$$

In this equation, n_m is the maximum number of adsorption sites on the surface of a particle per square centimeter [assumed here as 10^{15}, e.g., *Tabazadeh and Turco*, 1993], $N_{s,F,int}$ is the time-integrated average number concentration (molec. cm^{-3}-air) of gas F

adsorbed to surfaces of particles of all sizes during chemical time step h, and $N_{gF,t-h}$ (molec. cm^{-3}-air) is the number concentration of gas F at the beginning of the time step.

The time-integrated average number concentration of gas molecules adsorbed to particle surfaces is derived by first assuming that the time-rate of change of the number concentration (molec. cm^{-3}-air) on all surfaces is

$$\frac{dN_{s,F}(t)}{dt} = \frac{1}{4}\bar{v}_F a N_{g,F}(t) = \frac{1}{4}\bar{v}_F a\left[N_{g,F,t-h} - N_{s,F}(t)\right] \quad \text{(S3)}$$

where $N_{g,F}(t)=N_{g,F,t-h}-N_{s,F}(t)$ is the instantaneous gas-phase concentration of adsorbing species F. Integrating this equation gives the instantaneous number concentration of molecules on particle surfaces at time t after start of growth as

$$N_{s,F}(t) = N_{g,F,t-h}\left(1 - \exp^{-\bar{v}_F a t/4}\right) \quad \text{(S4)}$$

Further integrating the surface concentration over time step h and averaging over the time step gives the time-integrated average number concentration on surfaces as

$$N_{s,F,\text{int}} = \frac{1}{h}\int_0^h N_{s,F}(t)dt = N_{g,F,t-h}\left[1 - \frac{4}{\bar{v}_F a h}\left(1 - e^{-\bar{v}_F a h/4}\right)\right] \quad \text{(S5)}$$

Figure S2 shows a plot of $N_{s,F,int}$ / $N_{g,F,t-h}$ for HCl adsorption versus time step size at 190 K. As the surface area concentration decreases, the ratio decreases, which decreases the rate coefficient in Equation S2. The time step h is really the time interval during which chemistry is integrated over much smaller time steps in the model. Thus, for example, if h = 4 hours, chemistry is integrated during this period with time steps varying from 10^{-9} s to 900 s (with photolysis varying with these steps as well), but with surface coverage of the adsorbed species held constant and determined from Equation S5.

The use of Equation S2 assumes that molecules of gas *E* react with molecules of adsorbed gas *F* only on the surfaces of particles. After the reaction occurs, a gas product escapes and an adsorbed product remains. During the long model time interval (e.g., *h*=14,400 s), additional molecules of gas *F* adsorb to the surface on top of adsorbed products. The total number of layers of adsorbed gas *F* that can deposit on a surface during time step *h* is simply

$$L = \frac{N_{s,F,\mathrm{int}}}{a n_m} \tag{S6}$$

indicating that Equation S2 can be rewritten as

$$k_{s,E,F} = \frac{1}{4} \bar{v}_E \gamma_{E,F} a \frac{L}{N_{g,F,t-h}} \tag{S7}$$

However, the equation used in the model is Equation S2 combined with Equation S5, which yields the second-order rate coefficient (cm^3 $molec.^{-1}$ s^{-1}),

$$k_{s,E,F} = \frac{1}{4} \frac{\bar{v}_E \gamma_{E,F}}{n_m} \left[1 - \frac{4}{\bar{v}_F a h} \left(1 - e^{-\bar{v}_F a h / 4} \right) \right] \tag{S8}$$

The use of Equation S8 assumes that surface reactions occur only with newly adsorbed molecules *F* each time step *h*. This assumption appears reasonable as Equation S6 suggests multiple layers of gas are buried each time interval following reaction to a new adsorbed component.

In the model, chemical calculations were operator split from other processes for a time interval of four hours, during which SMVGEAR II solved chemistry using time steps varying between 10^{-9} and 900 s. Each time step was predicted based on the stiffness of the system, the relative error tolerance (set to 10^{-3}), and the absolute error tolerance (variable). With the second-order rate coefficient expression, Equation S8, all bimolecular heterogeneous reactions used could be solved conserving mass, assuming

reactants and products were in the gas phase. Aerosol and liquid heterogeneous reactions occurred on the aerosol and cloud liquid, distributions respectively. Water-ice and nitric acid trihydrate (NAT) reactions occurred on both the cloud ice and graupel distributions. Products were partitioned to the size-resolved aerosol or hydrometeor particle proportionally to the number of surface sites on each particle.

Radiative transfer was solved through gases, aerosol particles, clouds, sea ice, and snow [*Jacobson*, 2004, 2006]. Aerosols fed back to meteorology through their effects on radiation, clouds, the relative humidity, and pressure. For example, aerosol uptake of liquid water by hydration, calculated iteratively during internal aerosol equilibrium calculations in each size bin following nonequilibrium growth, modified the absolute humidity and temperature (due to latent heat exchange), both of which affected the relative humidity, which fed back to the rate of water uptake. Similarly, since precipitation and evaporation changed the amount of water vapor, which changed air pressure, changes in aerosols changed air pressure by changing cloud drop size and, therefore precipitation rates.

Ocean mixed-layer depths, velocities, temperatures, and energy and mass transport were predicted in time with a 2-D potential enstrophy-, kinetic energy-, and mass-conserving scheme, forced by wind stress [*Ketefian and Jacobson*, 2008]. Additional layers existed below each ocean mixed-layer grid cell to treat energy and chemical diffusion from the mixed layer to the deep ocean and ocean chemistry.

S3. Baseline Emissions. Table 1 of the main text shows global gas emissions from fossil fuel sources (including shipping and aircraft), biofuel burning, and biomass burning used in the model. Baseline global (1^{o}x1^{o} resolution) monthly emissions of NO_x, N_2O, CO, CO_2, SO_2, CH_4, and speciated organic gases from anthropogenic sources aside from shipping, aircraft, biofuel burning, and biomass burning, were obtained from *Olivier et al*. [1996]. Gas emissions from this dataset were originally for 1995, except that speciated

organics were for 1990 but scaled to 1995 by the 1995:1990 total nonmethane organic emission ratio since the 1995 organic gas inventory did not include speciation. Species not treated explicitly (e.g., alkanes, ethyne, trimethylbenzene) were split into carbon bond groups with splitting factors from *Carter* (http://pah.cert.ucr.edu/~carter/emitdb/).

The world CO_2 emission rate from onroad vehicles in 1995 was 3760 Tg-CO_2/yr [*Olivier et al*., 1996], or 15.2% of the total fossil-fuel carbon dioxide emitted that year. The carbon dioxide emission rate in 2004 was about 22% higher than in 1995 [*Marland et al*., 2006]. However, 1995 data were used for this study since most other emissions were from that year. The results found here for 1995 may be scalable to other years with different CO_2 emissions.

Emission of FFOV H_2 and H_2O were derived as follows. The mass emission ratio of H_2:CO from a FFOV was estimated as 0.0285 g-H_2/g-CO, the mean value from *Barnes et al*. [2003]. Although the reported uncertainty of this number was +/-12%, such uncertainty, and differences between *Barnes et al*. and other studies, which are up to about 33%, would have little impact on the results here since it was found that the primary influence on results was the reduction in fossil fuels, not hydrogen chemistry. The 1995 onroad vehicle emission rate of CO was 195.7 Tg-CO/yr [*Olivier et al*., 1996], giving a FFOV H_2 emission rate of 5.58 Tg-H_2/yr.

Water vapor emissions from FFOV were determined from the fleet-averaged gasoline plus diesel stoichiometric reaction $CH_{1.85}+1.4625\ O_2 \rightarrow CO_2+0.925\ H_2O$+energy [*Colella et al*., 2005]. Thus, while emitting 3760 Tg-CO_2/yr, FFOV simultaneously emitted 1424 Tg-H_2O/yr in 1995.

Natural and anthropogenic ammonia emissions were from *Bouwman et al*. [1997]. Natural emissions of biogenic isoprene, monoterpenes, other volatile organics, and nitric oxide; lightning NO and N_2O, ocean DMS, volcanic SO_2, CO_2 from bacterial and plant respiration (and CO_2 removal by photosynthesis) and CO_2 from ocean evaporation/dissolution were calculated during the model simulation as in *Jacobson and*

Streets [2008]. In addition natural H_2, CH_4, and N_2O emissions from soils and the oceans were treated, with emissions summarized in Table 1.

Table S3 summarizes the baseline black carbon (BC), primary organic carbon (POC), and sulfate emissions from aircraft, shipping, other fossil fuels, biofuels, and biomass burning used here. Fine BC and POC emissions from aircraft were obtained by applying emission factors of 0.038 g-BC/kg-fuel [*Petzold et al*., 1999] to fuel-use data [*Mortlock et al*., 1998; *Sutkus et al*., 2001] and assuming a POC:BC emission ratio of 1:1. Those from shipping were estimated by dividing the gridded, monthly sulfur shipping emission rate [*Corbett et al*. 1999] which totaled 4.24 Tg-S/yr, by 29.5 g-S/kg-fuel [*Corbett et al*., 2003, Table 1, for 1999 data] and multiplying the result by 1.02 g-BC-C/kg-fuel for shipping [*Bond et al*., 2004]. That for POC was obtained in the same manner, but by multiplying the result by 0.33 g-POC-C/kg-fuel [*Bond et al*., 2004]. Fine BC and POC for all other fossil-fuel sources (on- and nonroad vehicles, power sources, etc.) globally were obtained from *Bond et al*. [2004] after subtracting out shipping emissions. The totals from [*Bond et al*., 2004] before subtracting out such emissions were 3.040 Tg-BC-C/yr and 2.408 Tg-POC-C/yr. Fine biofuel-burning BC and POC emissions were obtained from *Bond et al*. [2004].

Natural plus anthropogenic biomass-burning particle and gas emissions were obtained by combining satellite-derived 8-day fuel burn data [*Giglio et al*., 2006] with landuse data (to determine fire type) and emission factors [*Andreae and Merlet*, 2002]. Fuel burn data for five separate years were used and repeated beyond five years in all simulations. It is generally estimated that about 90% of biomass-burning emissions today is anthropogenic. Coarse BC and POC aerosol particle emissions (not shown in Table S3) for all sources in the model were estimated as 25% and 45% those of fine BC and POC emissions, respectively. The POM:POC emission ratio used was 1.6:1 for fossil fuels and 2:1 for biofuel and biomass burning. The emission rate of S(VI) from fossil fuels was 1% that of BC+POM+S(VI).

Fossil-fuel components were emitted into the EFFS distribution. Biofuel- and biomass-burning components were emitted into the IM distribution. Gases (H_2, H_2O, NO, NO_2, N_2O, NH_3, SO_2, CO, CO_2, CH_4, CH_3OH, CH_3Cl, CH_3Br, C_2H_4, C_2H_6, C_3H_6, C_3H_8, HCHO, HCOOH, CH_3COOH, CH_3CHO, CH_3COCH_3, C_4H_6, C_5H_8, C_6H_6, C_6H_5CHO, $C_6H_5CH_3$, $C_6H_4CH_3CH_3$, and CH_3SCH_3) and other particle components (NH_4^+, Cl^-, SO_4^{2-}, NO_3^-, Na^+, K^+, Ca^{2+}, Mg^{2+}) from biomass and biofuel burning were obtained by multiplying BC biofuel or biomass emission rates by the ratio of the mean biofuel or biomass emission factor for each gas or particle component to that of BC from *Andreae and Merlet* [2001]. The ions K^+, Ca^{2+}, and Mg^{2+} were not carried in the simulations, but their mole-equivalent emissions were added to those of Na^+. Emissions of gases from shipping were obtained by scaling emission factors of individual gases to those of sulfur from the gridded inventory of *Corbett et al*. [2003], as described for particles above. Emissions of gases from aircraft were similarly obtained by applying emission factors to fuel use data from *Mortlock et al*. [1998] and *Sutkus et al*. [2001].

S4. WHFCV Emissions. For the WHFCV scenario, all onroad vehicles worldwide were converted to hydrogen fuel cell vehicles where the hydrogen was generated by wind electrolysis. Hydrogen was assumed to be produced in electrolyzers at local filling stations, and electricity for the electrolyzers was sent from wind farms to the filling station via transmission lines. Thus, no hydrogen pipelines or transport by vehicles was needed. Following electrolysis, the hydrogen was compressed and stored. Electricity for compression originated from the wind farms. Hydrogen was dispensed into vehicles at the stations.

The replacement of FFOV with WHFCV resulted in a reduction in emissions associated with FFOV and an increase in emissions associated with WHFCV. The only emissions associated with WHFCV were hydrogen leakage and chemically-produced water vapor (Table 1, main text). Fossil-fuel-related emissions due to the manufacture of

hydrogen fuel-cell vehicles, wind turbines, electrolyzers, and compressors were assumed to be offset by eliminating the manufacture of fossil-fuel vehicles, oil refineries, and oil wells and the transport of oil, diesel, and gasoline by trucks, trains, and ships although this is clearly a simplification.

Hydrogen leakage was assumed to occur during electrolysis of water, hydrogen compression, hydrogen storage at the filling station, vehicle fueling, in-vehicle hydrogen storage, in-vehicle flow through the fueling system, and hydrogen usage in the fuel cell stack. Studies have suggested a future hydrogen leakage rate of 3%, since the rate of natural gas leakage today is about 1% and that since hydrogen is a smaller molecule and more permeable than methane [*Schultz et al*., 2003; *Colella et al*., 2005]. Here, the leakage rate was similarly assumed to be 3%, the upper limit considered by *Zittel et al*. [1996] and *Shultz et al*. [2003]. This leakage rate is lower than that used in *Colella et al*. [2005], since they used a 10% leakage rate to ensure a conservative result, recognizing that the real leakage rate is most likely 1-3%. For this study, it was desired to calculate climate effects under a likely rather than conservative scenario. Because the major impacts found here were due almost exclusively to reductions in carbon dioxide and air pollution-precursor gases and particles rather than changes in hydrogen, a hydrogen leakage rate of 3 versus 10% does not impact the conclusions of this study.

The emission rate of hydrogen from leakage (kg-H_2/yr) was estimated here as

$$E_{H_2} = M_{H_2} \frac{f_L}{1 - f_L} \qquad \text{(S9)}$$

where f_L=0.03 is the fractional leakage rate and

$$M_{H_2} = \frac{V_{MT} \rho_G L_G \eta_G}{V_{MFG} G L_{H_2} \eta_{H_2}} \qquad \text{(S10)}$$

is the annual mass of hydrogen needed after leakage (kg-H_2/yr) to replace FFOV with WHFCV vehicles [*Colella et al*., 2005, Eq. 1]. In this equation, V_{MT} is the vehicle miles traveled per year (mi/yr), ρ_G is the density of gasoline (750 kg/m^3), L_G is the lower heating value of gasoline (44 MJ/kg), η_G is the tank-to-wheel efficiency of an average FFOV (0.16), V_{MPG} is the fleet averaged mileage of all onroad vehicles, including heavy and light-duty vehicles (17.11 mi/gal), G is 264.17287 gal/m^3, L_{H_2} is the lower heating value of hydrogen (120 MJ/kg), and η_{H_2} is the fleet-averaged tank-to-wheel efficiency of a WHFCV (0.46). These parameter values were justified in *Colella et al*. [2005].

In the present study, the leakage rate of hydrogen was determined in each grid cell by combining Equations S9 and S10 with a back-calculation of vehicle miles traveled from onroad transportation carbon dioxide emissions using

$$V_{MT} = \frac{E_{CO_2} m_C}{e_c m_{CO_2}} \qquad \text{(S11)}$$

where E_{CO_2} is the onroad FFOV carbon dioxide emission rate (kg-CO_2/yr) determined in each grid cell from emission data [*Olivier et al*., 1996], m_C is the molecular weight of carbon (12.011 g/mol), m_{CO_2} is the molecular weight of carbon dioxide (44.0098 g/mol), and e_c is the average emission rate of carbon per mile, selected as the 1999 U.S. fleet-averaged value of 0.140 kg-C/mi [*Colella et al*., 2005, Table 2].

Combining Equation S11 with the global vehicle CO_2 emission rate (Section S3) gives 7.33x10^{12} mi/yr traveled worldwide. U.S. onroad vehicles moved 2.68x10^{12} mi in 1999, suggesting that about 36% of the world's vehicle mileage was in the U.S. From Equation S10, the global hydrogen production rate to power all 1995 onroad vehicles worldwide is 155.7 Tg-H_2/yr. An additional 4.82 Tg-H_2/yr leaks (Equation S9), requiring a total production of 160.5 Tg-H_2/yr to account for leakage from and hydrogen consumption in WHFCV. For comparison, *Schultz et al*. [2003] estimated hydrogen leakage due to converting 50% of the world's fossil fuel combustion of approximately 10-15 Tg-H_2/yr assuming a 3% leakage rate. Scaling this number by 15.2% (the percent

of the world's fossil fuel used in vehicles - Section S3) / 50% (the percent of the world's fossil fuel converted in *Schultz et al.*) gives 3-4.6 Tg-H_2/yr, close to that derived here. *Tromp et al.* [2003] estimated hydrogen leakage (at a 10% leakage rate) from 100% of fossil fuel combustion of 60-120 Tg-H_2/yr. Scaling this number by (3% leakage / 10% leakage) * (15.2% / 100%) gives 2.7-5.5 Tg-H_2/yr, surrounding the estimate here. H_2 emissions from *Colella et al.* [2005], once scaled by differences in leakage rate (3% here versus 10% in that study) and vehicle miles traveled between the world in 1995 and U.S in 1999, yields the same emissions as here.

Whereas hydrogen leakage from WHFCV may increase H_2 emissions by 4.82 Tg-H_2/yr, the elimination of FFOV may reduce H_2 emissions by 5.58 Tg-H_2/yr (Section S3). Thus, switching to WHFCV may cause little change in H_2 emissions.

Water vapor emissions (kg-H_2O/yr) due to the fuel cell reaction $H_2 + 0.5O_2 \rightarrow H_2O$ + energy were calculated as

$$E_{H_2O} = M_{H_2} \frac{m_{H_2O}}{m_{H_2}} \quad \text{(S12)}$$

where m_{H_2O} and m_{H_2} are the molecular weights of water vapor (18.015 g/mol) and hydrogen (2.016 g/mol), respectively. With the hydrogen mass required here to operate vehicles (155.7 Tg-H_2/yr), global water vapor emissions from WHFCV were 1390 Tg-H_2O/yr. Water vapor emissions from FFOV were 1424 Tg-H_2O/yr (Section S3).

Whereas conversion to WHFCV may slightly reduce water vapor and hydrogen emissions relative to FFOV, such reductions are not statistically significant and could change sign with slight changes in assumptions. For example, WHFCV would emit more H_2 than FFOV if the leakage rate increased from 3.0 to 3.5%. As such, it can be concluded only that emissions of water vapor and hydrogen from WHFCV are effectively the same as those from FFOV they replace.

Table S3 shows black carbon, primary organic carbon, and sulfate emissions in the WHFCV scenario. BC, POC, and sulfate emissions all decreased in the WHFCV scenario relative to the baseline scenario.

S5. Additional Figures. Figure S1 shows modeled annually-averaged vertical profiles of the globally-averaged differences between parameters from the WHFCV and FFOV simulations. These figures are referred to in the main text only.

S6. Implications and Caveats. An important question to address for this study is the feasibility and unintended consequences of running the world's or U.S.' onroad vehicles on hydrogen produced by electrolysis from wind-generated electricity. A separate analysis [*Jacobson*, 2008] indicates that, if this were done in the U.S. in 2007, 229,000-428,000 5-MW wind turbines operating in locations where the wind speed is 8.5 m/s (low number of turbines) to 7.0 m/s (high number of turbines) would be needed. Such turbines would require about 1.1-2.1% of the 50 U.S. states, for turbine spacing, but only 3-8 square kilometers of land area for the turbine footprint on the ground. Almost all the area between turbine towers could be used for farming, ranching, fishing, or open space.

For comparison, wind-powered battery-electric vehicles (WBEV) would require about 3 times fewer 5 MW turbines to run the same vehicles: 73,000-144,000. The reason is that batteries are 75-86% efficient from plug to wheel, whereas WHFCV have three plug-to-wheel efficiency losses – electrolysis (about 74% efficient), compression (about 90% efficient), and the fuel cell (about 46-50% efficient) -- which together give a plug-to-wheel efficiency of about 30-33%. This is much lower than that of WBEV but higher than the tank-to-wheel efficiency of FFOV (around 16-18%). Replacing all U.S. onroad FFOV with WBEV would require an ocean and land area equivalent to 0.35-0.7 percent of the 50 U.S. states, for turbine spacing. The footprint on the ground to power onroad U.S. WBEV would be only 0.9-2.8 km^2 for the turbine towers.

The percentages of U.S. land required for turbine spacing in both cases (0.9-2.8% for WHFCV and 0.35-0.7% for WBEV) is much less than the 15% of U.S. land available that has wind speeds at 80 m that are fast enough for economical wind power production [*Archer and Jacobson*, 2005].

Whereas WHFCV emit water vapor and molecular hydrogen, WBEV do not emit either. The additional hydrogen and water vapor reduction by battery-electric vehicles powered by wind (WBEV) relative to WHFCV, though, should have little impact on stratospheric and tropospheric composition and climate since the changes in pollution-precursor gases and particles and carbon dioxide, which are similar for WBEV as for WHFCV in their lifecyle, dominate the effects of WHFCV versus FFOV.

The results here found for wind-powered HFCVs and BEVs should apply similarly to such vehicles powered by solar photovoltaic's, concentrated solar power, geothermal power, hydroelectric power, tidal power, and wave power, since these electric power sources have lifecycle emissions not significantly lower than those of wind turbines [*Jacobson*, 2008].

Wind turbines extract energy from the wind, reducing their speeds and increasing vertical velocities. However, if the entire world (electric plus nonelectric sources) were powered by 7.7 million 1.5 MW turbines, the combined energy loss from the slower winds among all wakes worldwide in the boundary layer (about 1 km) would be only about 0.05% [*Sta. Maria and Jacobson*, 2008].

S7. References

Andreae, M. O. and P. Merlet (2001), Emission of trace gases and aerosols from biomass burning, *Global Biogeochemical Cycles*, *15*, 955-966.

Archer, C.L., and M.Z. Jacobson (2005), Evaluation of global windpower, J. Geophys. Res. 110, D12110, doi:10.1029/2004JD005462.

Atkinson, R. (1997), Gas-phase tropospheric chemistry of volatile organic compounds, 1, Alkanes and alkenes, *J. Phys. Chem. Ref. Data, 26*, 215-290.

Atkinson, R., D.L. Baulch, R.A. Cox, et al. (1997), Evaluated kinetic, photochemical, and heterogeneous data for atmospheric chemistry. Supplement V., *J. Phys. Chem. Ref. Data*, *26*, 521-1011.

Bahta, A., R. Simonaitis, and J. Heicklen (1984), Reactions of ozone with olefins: Ethylene, allene, 1,3-butadiene, and trans-1,3-pentadiene, *Int. J. Chem. Kinetics, 16*, 1227-1246.

Barnes, D.H., S.C. Wofsy, B.P. Fehlau, E.W. Gottlieb, J.W. Elkins, G.S. Dutton, and P.C. Novelli (2003), Hydrogen in the atmosphere: Observations above a forest canopy in a polluted environment, *J. Geophys. Res., 108* (D6) doi:10.1029/2001JD001199.

Bond, T.C., Streets, D.G., Yarber, K.F., Nelson, S.M., Woo, J.-H. & Klimont, Z. (2004), A technology-based global inventory of black and organic carbon emissions from combustion, *J. Geophys. Res*., 109, D14203, doi: 10.1029/2003JD003697.

Bouwman, A. F., D. S. Lee, W. A. H. Asman, F. J. Dentener, K. W. van der Hoek, and J. G. J. Olivier (1997), A global high-resolution emission inventory for ammonia, *Global Biogeochem. Cycles*, *11*, 561-587.

Colella, W.C., M.Z. Jacobson, and D.M. Golden (2005), Switching to a U.S. hydrogen fuel cell vehicle fleet: The resultant change in emissions, energy use, and greenhouse gases, *J. Power Sources, 150*, 150-181.

Corbett, J.J., P.S. Fischbeck, and S.N. Pandis (1999), Global nitrogen and sulfur emissions inventories for oceangoing ships, *J. Geophys. Res., 104,* 3457-3470.

Corbett, J.J., and H.W. Koehler (2003), Updated emissions from ocean shipping, *J. Geophys. Res., 108* (D20), 4650, doi:10.1029/2003JD003751.

Drdla, K., M.R. Schoeberl, and E.V. Browell (2002a), Microphysical modeling of the 1999-2000 Arctic winter: 1. Polar stratospheric clouds, denitrification, and dehydration, *J. Geophys. Res., 107*, 8312, doi:10.1029/2001JD000782.

Drdla, K., and M.R. Schoeberl (2002b), Microphysical modeling of the 1999-2000 Arctic winter 2. Chlorine activation and ozone depletion, *J. Geophys. Res., 107*, 8319, doi:10.1029/2001JD001159.

Drdla, K., B.W. Gandrud, D. Baumgardner, J.C. Wilson, T.P. Bui, D. Hurst, S.M. Schauffler, H. Jost, J.B. Greenblatt, and C.R. Webster (2002c), *J. Geophys. Res., 107*, 8318, doi:10.1029/2001JD001127.

Gery, M. W., G.Z. Whitten, and J.P. Killus (1988), Development and testing of the CBM-IV for urban and regional modeling, Rep. EPA-600/3-88-012. U. S. Environmental Protection Agency, Research Triangle Park, NC.

Gery, M. W., G.Z. Whitten, J.P. Killus, and M.C. Dodge (1989), A photochemical kinetics mechanism for urban and regional scale computer modeling. *J. Geophys. Res., 94*, 12,925-12,956.

Giglio, L., G.R. van der Werf, J.T. Randerson, G.J. Collatz, and P. Kasibhatla (2006), Global estimation of burned area using MODIS active fire observations, *Atmos. Chem. and Physics, 6*, 957-974.

Griffin, R.J., D. Dabdub, and J.H. Seinfeld (2002), Secondary organic aerosol 1. Atmospheric chemical mechanism for production of molecular constituents, *J. Geophys. Res., 107*, (D17), 4332, doi:10.1029/2001JD000541.

Hanson, D., and K. Mauersberger (1988), Laboratory studies of the nitric acid trihydrate: Implications for the south polar stratosphere, *Geophys. Res. Lett., 15*, 855-858.

Jacobson, M.Z. (1997), Development and application of a new air pollution modeling system. Part III: Aerosol-phase simulations, Atmos. Environ., *31A*, 587-608.

Jacobson, M. Z. (1998), Improvement of SMVGEAR II on vector and scalar machines through absolute error tolerance control. *Atmos. Environ., 32*, 791–796.

Jacobson, M. Z. (2001a), GATOR-GCMM: A global through urban scale air pollution and weather forecast model. 1. Model design and treatment of subgrid soil, vegetation, roads, rooftops, water, sea ice, and snow., *J. Geophys. Res.*, *106*, 5385-5402.

Jacobson, M. Z. (2001b), GATOR-GCMM: 2. A study of day- and nighttime ozone layers aloft, ozone in national parks, and weather during the SARMAP Field Campaign, *J. Geophys. Res.*, *106*, 5403-5420.

Jacobson, M. Z., (2001c), Strong radiative heating due to the mixing state of black carbon in atmospheric aerosols, *Nature*, *409*, 695-697.

Jacobson, M. Z. (2002a), Analysis of aerosol interactions with numerical techniques for solving coagulation, nucleation, condensation, dissolution, and reversible chemistry among multiple size distributions, *J. Geophys. Res.*, *107* (D19), 4366, doi:10.1029/ 2001JD002044.

Jacobson, M. Z. (2002b), Control of fossil-fuel particulate black carbon plus organic matter, possibly the most effective method of slowing global warming, *J. Geophys. Res., 107*, (D19), 4410, doi:10.1029/ 2001JD001376.

Jacobson, M. Z. (2003), Development of mixed-phase clouds from multiple aerosol size distributions and the effect of the clouds on aerosol removal, *J. Geophys. Res.*, *108* (D8), 4245, doi:10.1029/2002JD002691.

Jacobson, M.Z. (2004), The climate response of fossil-fuel and biofuel soot, accounting for soot's feedback to snow and sea ice albedo and emissivity, *J. Geophys. Res.*, *109*, doi:10.1029/2004JD004945.

Jacobson, M.Z. (2005a), A solution to the problem of nonequilibrium acid/base gas-particle transfer at long time step, *Aerosol Sci. Technol, 39*, 92-103.

Jacobson, M.Z. (2005b), Fundamentals of Atmospheric Modeling, Second Edition, Cambridge University Press, New York, 813 pp.

Jacobson, M.Z. (2006), Effects of absorption by soot inclusions within clouds and precipitation on global climate, *J. Phys. Chem., 110*, 6860-6873.

Jacobson, M.Z. (2008) Review of solutions to global warming, air pollution, and energy security, *Energy and Environmental Science*, in review, www.stanford.edu/group/efmh/jacobson/revsolglobwarmairpol.htm.

Jacobson, M. Z., J. H. Seinfeld, G. R. Carmichael, and D.G. Streets, The effect on photochemical smog of converting the U.S. fleet of gasoline vehicles to modern diesel vehicles, *Geophys. Res. Lett.*, *31*, L02116, doi:10.1029/2003GL018448, 2004.

Jacobson, M.Z., W.C. Colella, and D.M. Golden (2005), Cleaning the air and improving health with hydrogen fuel cell vehicles, Science, 308, 1901-1905.

Jacobson, M.Z., and Y.J. Kaufman (2006), Wind reduction by aerosol particles. *Geophys. Res. Letters*, *33* (24), doi:10.1029/2006GL027838.

Jacobson, M.Z., Y.J. Kaufmann, Y. Rudich (2007), Examining feedbacks of aerosols to urban climate with a model that treats 3-D clouds with aerosol inclusions, *J. Geophys. Res., 112*, D24205, doi:10.1029/2007JD008922.

Jacobson, M.Z., and D.G. Streets (2008), The influence of future anthropogenic emissions on climate, natural emissions, and air quality, in review.

Jensen, E.J., O.B. Toon, A. Tabazadeh, and K. Drdla (2002), Impact of polar stratospheric cloud particle composition, number density, and lifetime on denitrification, *J. Geophys. Res., 107*, 8284, doi:10.1029/2001JD000440.

Ketefian G., and Jacobson M.Z (2008), A mass, energy, vorticity, and potential enstrophy conserving boundary treatment scheme for the shallow water equations, *J. Comp. Phys.*, in press, www.stanford.edu/group/efmh/gsk/.

Lin, J.-S., and A. Tabazadeh (2001), A parameterization of an aerosol physical chemistry model for the $NH_3/H_2SO_4/HNO_3/H_2O$ system at cold temperatures, *J. Geophys. Res., 106*, 4815-4829.

Marland, G., T.A. Boden, and R.J. Andres (2006), http://cdiac.ornl.gov/trends/emis/em_cont.htm (2006). 2003 data extrapolated to 2005 using the slope of the carbon emission change per year.

Mortlock, A.M., and R. Van Alstyne (1998), Military, Charter, Unreported Domestic Traffic and Gen. Aviation: 1976, 1984, 1992, and 2015 Emission Scenarios, NASA CR- 1998-207639,, http://ntrs.nasa.gov/archive/nasa/casi.ntrs.nasa.gov/19980047346_1998120131.pdf.

Olivier, J. G. J., A. F. Bouwman, C. W. M. Van der Maas, J. J. M. Berdowski, C. Veldt, J. P. J. Bloos, A. J. H. Visschedijk, P. Y. J. Zandveld, and J. L. Haverlag (1996), Description of EDGAR Version 2.0: A set of global emission inventories of greenhouse gases and ozone-depleting substances for all anthropogenic and most natural sources on a per country basis on 1°x1° grid, National Institute of Public Health and the Environment, RIVM) report no. 771060 002 / TNO-MEP report no. R96/119.

Paulson, S. E. and J.H. Seinfeld (1992), Development and evaluation of a photooxidation mechanism for isoprene. *J. Geophys. Res*, *97*, 20,703-20,715.

Petzold, A., A. Dopelheuer, C.A. Brock, and F. Schroder (1999), In situ observations and model calculations of black carbon emission by aircraft at cruise altitude, *J. Geophys. Res., 104*, 22,171-22,181.

Robinson, G.N., D.R. Worsnop, J.T. Jayne, C.E. Kolb, and P. Davidovits (1997), Heterogeneous uptake of $ClONO_2$ and N_2O_5 by sulfuric acid solutions, *J. Geophys. Res., 102*, 3583-3602.

Sander, S.P., R.R. Friedl, D.M. Golden, M.J. Kurylo, G.K. Moortgat, H. Keller-Rudek, P.H. Wine, A.R. Ravishankara, C.E. Kolb, M.J. Molina, B.J. Finlayson-Pitts, R.E. Huie, and V.L. Orkin (2006), Chemical kinetics and photochemical data for use in atmospheric studies, Evaluation Number 15, JPL Publication No. 06-2.

Schultz, M.G., T. Diehl, G.P. Brasseur, and W. Zittel (2003), Air pollution and climate-forcing impacts of a global hydrogen economy, Science, 302, 624-627.

Shi, Q., J.T. Jayne, C.E. Kolb, D.R. Worsnop, and P. Davidovits (2001), Kinetic model for reaction of ClONO2 with H2O and HCl and HOCl with HCl in sulfuric acid solutions, *J. Geophys. Res., 106* (D20), 24,259-24,274.

Sta. Maria, M., and M.Z. Jacobson (2008), New parameterization for wind farm effects on the atmosphere. Proc. AWEA Wind Power 2008 Conference, Houston, Texas, June 1-4, 2008, CD-ROM.

Strawa, A.W., K. Drdla, M. Fromm, R.F. Pueschel, K.W. Hoppel, E.V. Browell, P. Hamill, and D.P. Dempsey (2002), Discriminating Types Ia and Ib polar stratospheric clouds in POAM satellite data, *J. Geophys. Res., 107*, 8291, doi:10.1029/2001JD000458.

Sutkus, D.J., S.L. Baughcum, and D.P. DuBois (2001), Scheduled Civil Aircraft Emission Inventories for 1999: Database Development and Analysis, NASA/CR-2001-211216, http://gltrs.grc.nasa.gov/reports/2001/CR-2001-211216.pdf.

Tabazadeh, A., and R.P. Turco (1993), A model for heterogeneous chemical processes on the surfaces of ice and nitric acid trihydrate particles, *J. Geophys. Res., 98* 12,727-12,740.

Toon, O.B., P. Hamill, R.P. Turco, and J. Pinto (1986), Condensation of HNO3 and HCl in the winter polar stratospheres, *Geophys. Res. Lett. Nov. Supp., 13*, 1284-1287.

Tromp, T.K., R.-L. Shia, M. Allen, J.M. Eiler, and Y.L. Yung (2003), Potential environmental impact of a hydrogen economy on the stratosphere, *Science, 300*, 1740-1742.

Turco, R.P., O.B. Toon, and P. Hamill (1989), Heterogeneous physiochemistry of the polar ozone hole, *J. Geophys. Res., 94*, 16,493-16,510.

Worsnop, D.R., L.E. Fox, M.S. Zahniser, and S.C. Wofsy (1993), Vapor pressures of solid hydrates of nitric acid: Implications for polar stratospheric clouds, *Science, 259*, 71-74.

Yin, F., D. Grosjean, and J.H. Seinfeld (1990), Photooxidation of dimethyl sulfide and dimethyl disulfide. I: Mechanism development. *J. Atmos. Chem.*, *11*, 309-64.

Zhang, R., P.J. Wooldridge, J.P.D. Abbatt, and M.J. Molina (1993), Physical chemistry of the H2SO4/H2O binary system at low temperatures: stratospheric implications, *J. Phys. Chem., 97*, 7351-7358.

Zittel., W., M. Altmann, and L-B-S. GmbH (1996), Molecular hydrogen and water vapour emissions in a global hydrogen economy, Proc. 11th World Hydrogen Energy Conf., T.N. Veziroglu, C.J. Winter, J.P. Baelt, G. Kreysa, eds., Schon and Wetzel, Frankfurt, Germany, www.hydrogen.org/Knowledge/Vapour.htm.

Table S1. Aerosol and hydrometeor size distributions treated in the model and the parameters (number concentration and chemical mole concentrations) present in each size bin of each size distribution.

Aerosol Emitted Fossil-Fuel Soot (EFFS)	Aerosol Internally Mixed (IM)	Cloud / Precipitation Liquid	Cloud / Precipitation Ice	Cloud / Precipitation Graupel
Number	Number	Number	Number	Number
BC	BC	BC	BC	BC
POM	POM	POM	POM	POM
SOM	SOM	SOM	SOM	SOM
H_2O(l)-hydrated	H_2O(aq)-hydrated	H_2O(aq)-hydrated	H_2O(aq)-hydrated	H_2O(aq)-hydrated
H_2SO_4(aq)	H_2SO_4(aq)	H_2SO_4(aq)	H_2SO_4(aq)	H_2SO_4(aq)
HSO_4^-	HSO_4^-	HSO_4^-	HSO_4^-	HSO_4^-
SO_4^{2-}	SO_4^{2-}	SO_4^{2-}	SO_4^{2-}	SO_4^{2-}
NO_3^-	NO_3^-	NO_3^-	NO_3^-	NO_3^-
Cl^-	Cl^-	Cl^-	Cl^-	Cl^-
H^+	H^+	H^+	H^+	H^+
NH_4^+	NH_4^+	NH_4^+	NH_4^+	NH_4^+
NH_4NO_3(s)	NH_4NO_3(s)	NH_4NO_3(s)	NH_4NO_3(s)	NH_4NO_3(s)
$(NH4)_2SO_4$(s)	$(NH4)_2SO_4$(s)	$(NH4)_2SO_4$(s)	$(NH4)_2SO_4$(s)	$(NH4)_2SO_4$(s)
	Na^+ (K^+,Mg^{2+},Ca^{2+})	Na^+ (K^+,Mg^{2+},Ca^{2+})	Na^+ (K^+,Mg^{2+},Ca^{2+})	Na^+ (K^+,Mg^{2+},Ca^{2+})
	Soildust	Soildust	Soildust	Soildust
	Pollen/spores/bact.	Pollen/spores/bact.	Pollen/spores/bact.	Pollen/spores/bact.
		H_2O(aq)-condensed	H_2O(s)	H_2O(s)

POM is primary organic matter; SOM is secondary organic matter. H_2O(aq)-hydrated is liquid water hydrated to electrolytes in solution. H_2O(aq)-condensed is condensed water. Condensed and hydrated water existed in the same particles. If condensed water evaporated, hydrated water and other aerosol material remained. H_2O(s) is liquid water that froze or water vapor that deposited as ice. Emitted species in the fossil-fuel soot distribution included BC, POM, H_2SO_4(aq), HSO_4^-, and SO_4^{2-}. The remaining species in the distribution formed by gas-to-particle conversion or crystallization. Sea spray, soildust, biomass burning, biofuel burning, pollen, spores, and bacteria were emitted into the internally-mixed distribution. Emitted species in sea spray included H_2O, Na^+, K^+, Mg^{2+}, Ca^{2+}, Cl^-, NO_3^-, H_2SO_4(aq), HSO_4^-, and SO_4^{2-}. Those in biomass and biofuel burning included the same plus BC and POM. In both cases, K^+, Mg^{2+}, Ca^{2+} were treated as equivalent Na^+. Pollen, spores, and bacteria were emitted into the same species. Homogenously nucleated species (H_2O, H_2SO_4(aq), HSO_4^-, SO_4^{2-}. NH_4^+) entered the IM distribution. Condensing gases on both aerosol distributions included H_2SO_4 and SOM. Dissolving gases on both aerosol distributions included HNO_3, HCl, and NH_3. All gases dissolved in liquid hydrometeor particles according to their effective Henry's constant. All aerosol and hydrometeor distributions were affected by self-coagulation and heterocoagulation to other distributions.

Table S2. Simulation- and globally-averaged values from the baseline simulation (with FFOV) and percent differences between the WHFCV ("wind") and baseline simulations.

Parameter	Baseline	Wind-base % Diff.	Parameter	Baseline	Wind-base % Diff.
Surface air temp. (K)	287.6	-0.0017	Benzene (mg/m^2)	6.1	-2.5
Surface albedo	0.195	+0.20	Toluene (mg/m^2)	0.87	-12.2
Cloud optical depth	4.82	-1.7	Isoprene (mg/m^2)	4.0	+10.2
Cloud liquid (kg/m^2)	0.015	-0.98	Monoterpenes (mg/m^2)	0.29	+5.0
Cloud ice (kg/m^2)	0.0043	-1.3	SO_2 (mg/m^2)	0.90	+0.89
Activated CCN (No cm^{-2})	2.93	-2.6	NH_3 (mg/m^2)	0.23	+2.8
Activated IDN (No cm^{-2})	0.067	-7.9	HCl (mg/m^2)	1.2	+0.66
Cloud fraction	0.567	-0.04	$ClONO_2$ (mg/m^2)	0.33	+2.2
Precipitation (mm/day)	2.68	+0.35	HOCl (mg/m^2)	0.25	-1.8
Surface wind speed (m/s)	5.92	-0.042	ClO (mg/m^2)	0.30	+1.2
Ocean pH	7.86	+0.021	Cl_2 (mg/m^2)	0.009	-8.5
Surf. thermal-IR (W/m^2)	-70.1	+0.28	BrO (mg/m^2)	0.018	+3.3
Surface solar (W/m^2)	170	+0.32	PM BC ($mg\text{-}BC/m^2$)	0.21	-6.7
Surface UV (W/m^2)	9.74	+0.86	PM POM ($mg\text{-}POM/m^2$)	1.3	-1.8
Aerosol optical depth	0.23	-3.8	PM SOM ($mg\text{-}SOM/m^2$)	7.4	-6.1
CO_2 (kg/m^2)	6.2	-0.46	PM H_2O (mg/m^2)	52	-2.5
H_2O (kg/m^2)	28.3	+0.22	PM S(VI) ($mg\text{-}SO_4^{2-}/m^2$)	2.7	-2.7
H_2 (mg/m^2)	898	-0.77	PM NO_3^- (mg/m^2)	0.9	-18.6
NO (mg/m^2)	0.28	-8.8	PM Cl^- (mg/m^2)	1.9	-0.42
NO_2 (mg/m^2)	0.78	-11	PM H^+ (mg/m^2)	0.025	-4.4
HNO_3 (mg/m^2)	5.8	-1.6	PM NH_4^+ (mg/m^2)	0.33	-1.7
OH (mg/m^2)	0.0067	-0.58	PM NH_4NO_3 (mg/m^2)	0.77	-9.5
O_3 (mg/m^2)	6300	+0.41	PM $(NH4)_2SO_4$ (mg/m^2)	0.50	+6.3
Surface O_3 (ppbv)	16.6	-6.2	PM Na^+ (mg/m^2)	1.8	-1.0
PAN (mg/m^2)	12.5	-11.6	PM Soil dust (mg/m^2)	140	-2.6
CO (mg/m^2)	5130	-4.8	PM Pol/spor/bact (mg/m^2)	0.67	-0.79
CH_4 (mg/m^2)	10,200	+0.25	PM_{tot} (mg/m^2)	204	-2.8
HCHO (mg/m^2)	4.0	-3.9	Surface $PM_{2.5}$ ($\mu g/m^3$)	47.8	-2.6
CH_3CHO (mg/m^2)	21.9	-1.6	Surface PM_{10} ($\mu g/m^3$)	137	-1.6

Divide mg/m^2 by 1.9637 to obtain Tg. Masses are of total chemical. UV=ultraviolet. PM=particulate matter of all sizes. PM_{10}=PM<10μm diameter. CCN=cloud condensation nuclei. IDN=ice deposition nuclei.

Table S3. Fine-particle global emission rates of black carbon (BC) (Tg-C/yr), primary organic carbon (POC) (Tg-C/yr), and S(VI) (Tg-SO_4/yr) for the baseline and WHFCV scenarios.

	(a) Aircraft	(b) Shipping	(c) All other Fossil Fuel	(d) Total Fossil Fuel (a+b+c)	(e) Biofuel	(f) Biomass burning	(g) Total (d+e+f)
BC Baseline	0.0062	0.147	3.029	3.182	1.634	2.806	7.622
BC WHFCV	0.0062	0.147	2.423	2.576	1.634	2.806	7.016
POC Baseline	0.0062	0.047	2.371	2.424	6.490	24.12	33.03
POC WHFCV	0.0062	0.047	1.897	1.950	6.490	24.12	32.55
S(VI) Baseline	0.00082	0.0069	0.030	0.0377	1.52	0.58	2.138
S(VI) WHFCV	0.00082	0.0069	0.024	0.0317	1.52	0.58	2.132

Data sources and sulfate/other emissions associated with these sources are described in the text.

Figure S1: Modeled annually-averaged vertical profiles of the globally-averaged differences and percent differences between parameters from the WHFCV and FFOV simulations. These figures are referred to in the main text only.

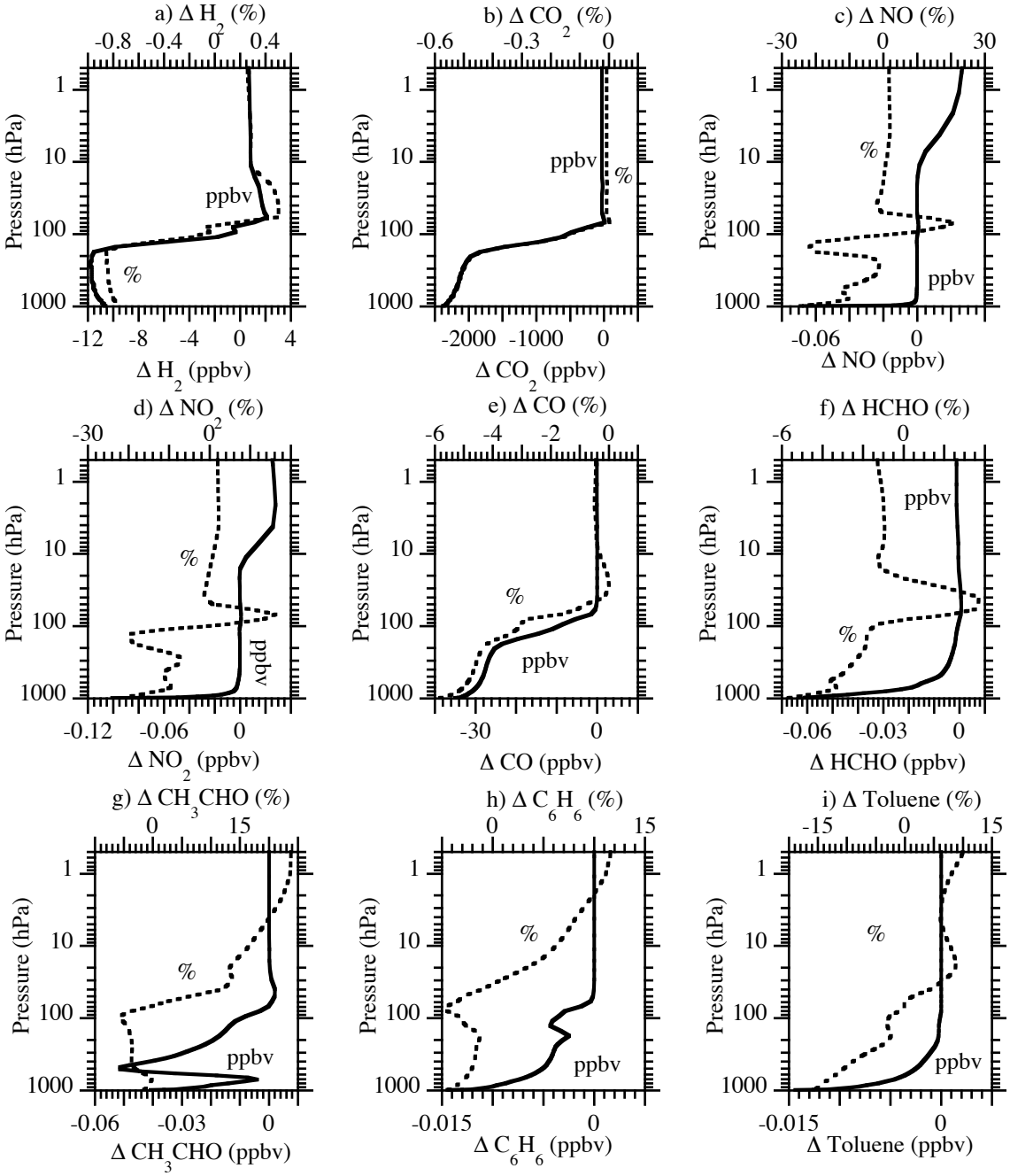

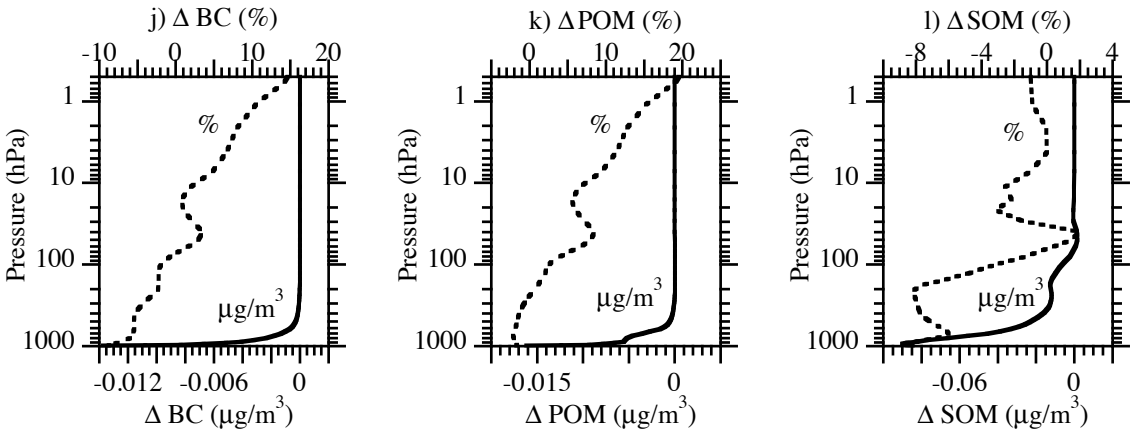
j) Δ BC (%)
k) Δ POM (%)
l) Δ SOM (%)
Pressure (hPa)
%
μg/m3
Δ BC (μg/m3)
Δ POM (μg/m3)
Δ SOM (μg/m3)

1

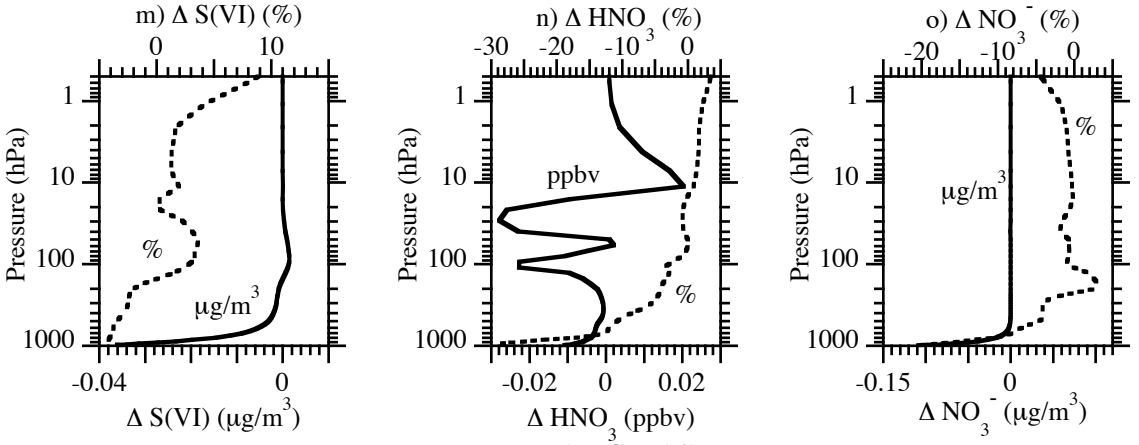
m) Δ S(VI) (%)
n) Δ HNO3 (%)
o) Δ NO3- (%)
Pressure (hPa)
ppbv
%
μg/m3
Δ S(VI) (μg/m3)
Δ HNO3 (ppbv)
Δ NO3- (μg/m3)

2

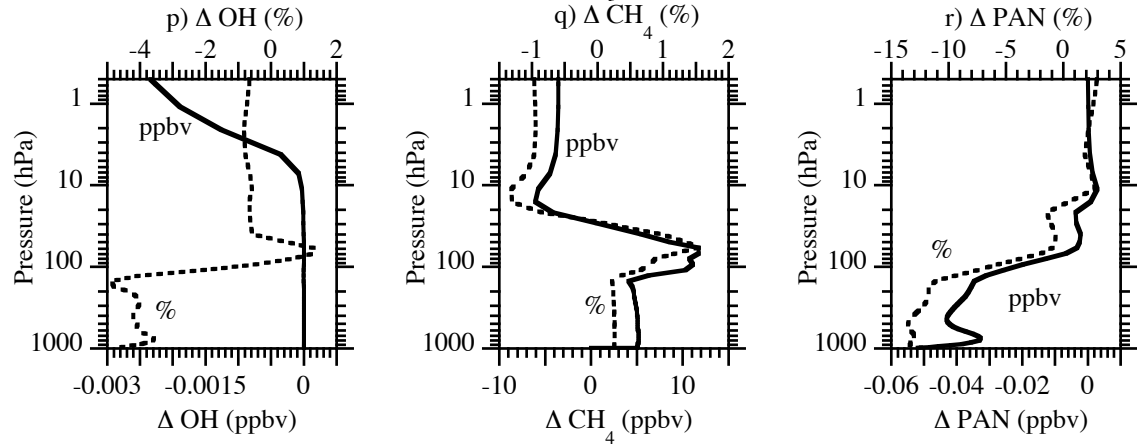
p) Δ OH (%)
q) Δ CH4 (%)
r) Δ PAN (%)
Pressure (hPa)
ppbv
%
Δ OH (ppbv)
Δ CH4 (ppbv)
Δ PAN (ppbv)

3

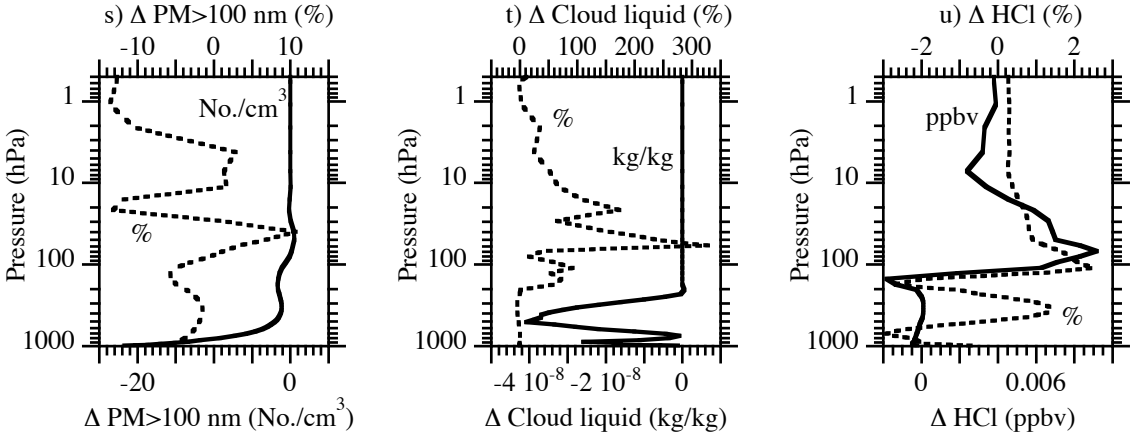
s) Δ PM>100 nm (%)
t) Δ Cloud liquid (%)
u) Δ HCl (%)
Pressure (hPa)
No./cm3
%
kg/kg
ppbv
Δ PM>100 nm (No./cm3)
Δ Cloud liquid (kg/kg)
Δ HCl (ppbv)

4

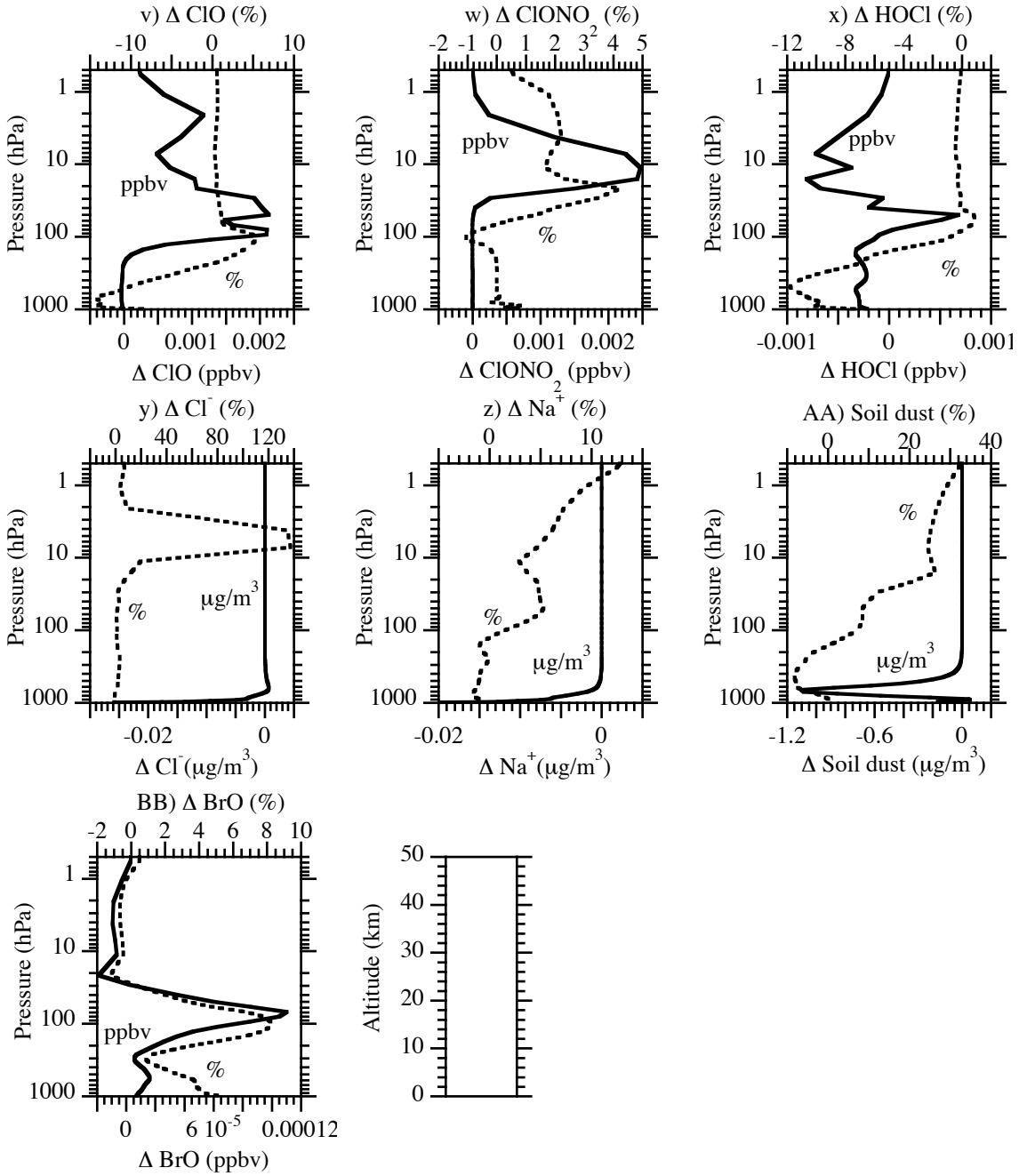
v) Δ ClO (%)
-10 0 10
Pressure (hPa)
1 10 100 1000
ppbv
%
0 0.001 0.002
Δ ClO (ppbv)
w) Δ ClONO2 (%)
-2 -1 0 1 2 3 4 5
ppbv
%
0 0.001 0.002
Δ ClONO2 (ppbv)
x) Δ HOCl (%)
-12 -8 -4 0
ppbv
%
-0.001 0 0.001
Δ HOCl (ppbv)
y) Δ Cl- (%)
0 40 80 120
%
μg/m3
-0.02 0
Δ Cl-(μg/m3)
z) Δ Na+ (%)
0 10
%
μg/m3
-0.02 0
Δ Na+(μg/m3)
AA) Soil dust (%)
0 20 40
%
μg/m3
-1.2 -0.6 0
Δ Soil dust (μg/m3)
BB) Δ BrO (%)
-2 0 2 4 6 8 10
ppbv
%
0 6 10-5 0.00012
Δ BrO (ppbv)
Altitude (km)
0 10 20 30 40 50

Figure S2. Ratio of the time-integrated average number concentration of molecules adsorbed to particle surfaces to the initial number concentration of molecules in the gas phase as a function of time step size h, obtained from Equation S5, for three values of surface area concentration, a (cm^2-particles cm^{-3}-air). T=190 K and m_F=36.46 g/mol (HCl), giving a thermal speed of 33,216 cm/s.

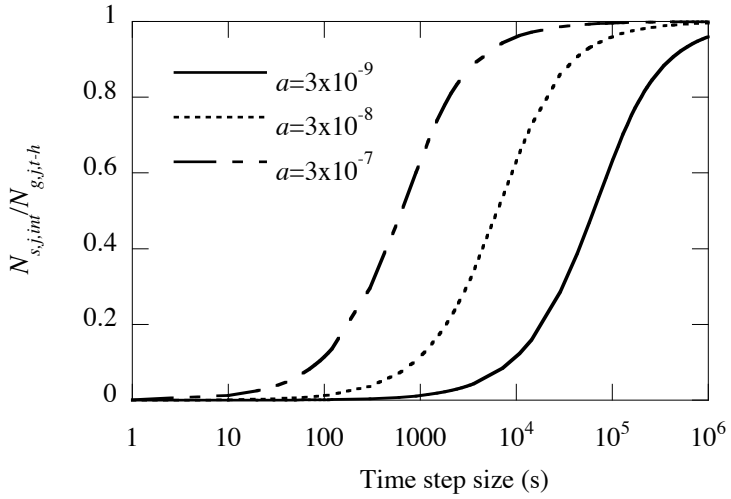

Reaction List. Gas-phase chemical kinetic reactions, reaction rate coefficients, and photoprocesses, and heterogeneous reactions treated in the model.

No.	Kinetic Reaction	F_c [a]	Rate Coefficient (s^{-1}, $cm^3\ s^{-1}$, or $cm^6\ s^{-1}$)	Ref.[b]
	Inorganic Chemistry			
1	$O + O_2 + M \rightarrow O_3 + M$		$6.00\times10^{-34}\ (300/T)^{2.3}$	A
2	$O + O_3 \rightarrow 2\ O_2$		$8.00\times10^{-12}\ e^{-2060/T}$	A
3	$O(^1D) + O_3 \rightarrow 2O_2$		1.20×10^{-10}	A
4	$O(^1D) + O_3 \rightarrow O_2 + 2O$		1.20×10^{-10}	A
5	$O(^1D) + O_2 \rightarrow O + O_2$		$3.30\times10^{-11}\ e^{55/T}$	A
6	$O(^1D) + N_2 \rightarrow O + N_2$		$2.15\times10^{-11}\ e^{110/T}$	A
7	$O(^1D) + CO_2 \rightarrow O + CO_2$		$7.50\times10^{-11}\ e^{115/T}$	A
8	$O(^1D) + N_2 + M \rightarrow N_2O + M$		$2.80\times10^{-36}\ (300/T)^{0.9}$	A
9	$O(^1D) + N_2O \rightarrow N_2 + O_2$		$4.90\times10^{-11}\ e^{20/T}$	A
10	$O(^1D) + N_2O \rightarrow NO + NO$		$6.70\times10^{-11}\ e^{20/T}$	A
11	$O(^1D) + H_2 \rightarrow OH + H$		1.10×10^{-10}	A
12	$O(^1D) + H_2O \rightarrow OH + OH$		$1.63\times10^{-10}\ e^{60/T}$	A
13	$H + O_2 \xrightarrow{M} HO_2$	(P) 0.6	$4.40\times10^{-32}\ (300/T)^{1.3}$ $4.70\times10^{-11}\ (300/T)^{0.2}$	A
14	$H + O_3 \rightarrow O_2 + OH$		$1.40\times10^{-10}\ e^{-470/T}$	A
15	$H + HO_2 \rightarrow H_2 + O_2$		5.67×10^{-12}	A
16	$H + HO_2 \rightarrow OH + OH$		7.29×10^{-11}	A
17	$H + HO_2 \rightarrow H_2O + O$		2.43×10^{-12}	A
18	$OH + O \rightarrow H + O_2$		$2.20\times10^{-11}\ e^{120/T}$	A
19	$OH + O_3 \rightarrow HO_2 + O_2$		$1.70\times10^{-12}\ e^{-940/T}$	A
20	$OH + H_2 \rightarrow H_2O + H$		$2.8\times10^{-12}\ e^{-1800/T}$	A
21	$OH + OH \rightarrow H_2O + O$		$1{,}80\times10^{-12}$	A
22	$OH + OH \xrightarrow{M} H_2O_2$	(P) 0.6	$6.90\times10^{-31}\ (300/T)^{0.8}$ 2.6×10^{-11}	A
23	$OH + HO_2 \rightarrow H_2O + O_2$		$4.80\times10^{-11}\ e^{250/T}$	A
24	$OH + H_2O_2 \rightarrow HO_2 + H_2O$		1.80×10^{-12}	A
25	$OH + NO \xrightarrow{M} HONO$	(P) 0.6	$7.00\times10^{-31}\ (300/T)^{2.6}$ $3.60\times10^{-11}\ (300/T)^{0.1}$	A
26	$OH + NO_2 \xrightarrow{M} HNO_3$	(P) 0.6	$1.80\times10^{-30}\ (300/T)^{3.0}$ 2.80×10^{-11}	A
27	$OH + NO_3 \rightarrow HO_2 + NO_2$		2.20×10^{-11}	A
28	$OH + HONO \rightarrow H_2O + NO_2$		$1.80\times10^{-11}\ e^{-390/T}$	A
29	$OH + HNO_3 \rightarrow H_2O + NO_3$		c	A
30	$OH + HO_2NO_2 \rightarrow H_2O + NO_2 + O_2$		$1.30\times10^{-12}\ e^{380/T}$	A
31	$OH + CO \rightarrow HO_2 + CO_2$		d	A
32	$HO_2 + O \rightarrow OH + O_2$		$3.00\times10^{-11}\ e^{200/T}$	A
33	$HO_2 + O_3 \rightarrow OH + 2O_2$		$1.40\times10^{-14}\ e^{-490/T}$	A
34	$HO_2 + HO_2 \rightarrow H_2O_2 + O_2$		e	A
35	$HO_2 + NO \rightarrow OH + NO_2$		$3.50\times10^{-12}\ e^{250/T}$	A
36	$HO_2 + NO_2 \xrightarrow{M} HO_2NO_2$	(P) 0.6	$2.00\times10^{-31}\ (300/T)^{3.4}$ $2.90\times10^{-12}\ (300/T)^{1.1}$	A
37	$HO_2NO_2 \xrightarrow{M} HO_2 + NO_2$		$k_{36} / (2.10\times10^{-27} \times e^{10900/T})$	

38	$HO_2 + NO_3 \rightarrow HNO_3 + O_2$		3.50×10^{-12}	A
39	$H_2O_2 + O \rightarrow OH + HO_2$		$1.40 \times 10^{-12}\, e^{-2000/T}$	A
40	$NO + O \xrightarrow{M} NO_2$	(P) 0.6	$9.00 \times 10^{-32}\, (300/T)^{1.5}$ 3.00×10^{-11}	A
41	$NO + O_3 \rightarrow NO_2 + O_2$		$3.00 \times 10^{-12} e^{-1500/T}$	A
42	$NO_2 + O \rightarrow NO + O_2$		$5.60 \times 10^{-12} e^{180/T}$	A
43	$NO_2 + O \xrightarrow{M} NO_3$	(P) 0.6	$2.50 \times 10^{-31}\, (300/T)^{1.8}$ $2.20 \times 10^{-11}\, (300/T)^{0.7}$	A
44	$NO_2 + O_3 \rightarrow NO_3 + O_2$		$1.20 \times 10^{-13}\, e^{-2450/T}$	A
45	$NO_3 + O \rightarrow NO_2 + O_2$		1.00×10^{-11}	A
46	$NO_3 + NO \rightarrow 2\ NO_2$		$1.50 \times 10^{-11}\, e^{170/T}$	B
47	$NO_3 + NO_2 \xrightarrow{M} N_2O_5$	(P) 0.6	$2.00 \times 10^{-30}\, (300/T)^{4.4}$ $1.40 \times 10^{-12}\, (300/T)^{0.7}$	A
48	$N_2O_5 \xrightarrow{M} NO_3 + NO_2$		$K_{47} / (3.00 \times 10^{-27} \times e^{10990/T})$	A
49	$N_2O_5 + H_2O \rightarrow 2\ HNO_3$		2.00×10^{-21}	B
	Organic Chemistry			
	Alkane, Alkene, and Aldehyde Chemistry			
50	$CH_4 + O(^1D) \rightarrow CH_3O_2 + OH$		1.50×10^{-10}	A
51	$CH_4 + O(^1D) \rightarrow CH_3O + H$		3.00×10^{-11}	B
52	$CH_4 + O(^1D) \rightarrow HCHO + H_2$		7.00×10^{-12}	B
53	$CH_4 + OH \rightarrow CH_3O_2 + H_2O$		$2.45 \times 10^{-12}\, e^{-1775/T}$	A
54	$CH_3O + O_2 \rightarrow HCHO + HO_2$		$3.90 \times 10^{-14}\, e^{-900/T}$	A
55	$CH_3O + NO \rightarrow HCHO + HO_2 + NO$		8.00×10^{-12}	A
56	$CH_3O + NO \xrightarrow{M} CH_3ONO$	(P) 0.6	$2.30 \times 10^{-29}\, (300/T)^{2.8}$ $3.80 \times 10^{-11}\, (300/T)^{0.6}$	A
57	$CH_3O + NO_2 \xrightarrow{M} CH_3ONO_2$	(P) 0.6	$5.30 \times 10^{-29}\, (300/T)^{4.4}$ $1.90 \times 10^{-11}\, (300/T)^{1.8}$	A
58	$CH_3ONO_2 + OH \rightarrow HCHO + NO_2 + H_2O$		$5.00 \times 10^{-13}\, e^{810/T}$	A
59	$CH_3O_2 + HO_2 \rightarrow CH_3OOH + O_2$		$4.10 \times 10^{-13}\, e^{750/T}$	A
60	$CH_3O_2 + NO \rightarrow CH_3O + NO_2$		$2.80 \times 10^{-12}\, e^{300/T}$	A
61	$CH_3O_2 + NO_2 \xrightarrow{M} CH_3O_2NO_2$	(P) 0.6	$1.00 \times 10^{-30}\, (300/T)^{4.8}$ $7.20 \times 10^{-12}\, (300/T)^{2.1}$	A
62	$CH_3O_2NO_2 \xrightarrow{M} CH_3O_2 + NO_2$		$k_{61} / (1.30 \times 10^{-28} \times e^{11200/T})$	A
63	$CH_3O_2 + CH_3O_2 \rightarrow 2\ CH_3O + O_2$		$5.90 \times 10^{-13}\, e^{-509/T}$	B
64	$CH_3O_2 + CH_3O_2 \rightarrow HCHO + CH_3OH$		$7.04 \times 10^{-14}\, e^{365/T}$	B
65	$CH_3O_2 + CH_3C(O)OO \rightarrow CH_3O_2 + CH_3O + CO_2$		$2.00 \times 10^{-12} e^{500/T}$	A
66	$CH_3O_2 + CH_3C(O)OO \rightarrow CH_3COOH + HCHO + O_2$		$2.20 \times 10^{-13} e^{500/T}$	B
67	$CH_3COOH + OH \rightarrow CH_3O_2 + CO_2 + H_2O$		$4.00 \times 10^{-13} e^{200/T}$	A
68	$CH_3OOH + OH \rightarrow CH_3O_2 + H_2O$		$3.80 \times 10^{-12}\, e^{200/T}$	A
69	$C_2H_6 + OH \rightarrow C_2H_5O_2 + H_2O$		$8.70 \times 10^{-12}\, e^{-1070/T}$	A
70	$C_2H_5O_2 + NO \rightarrow C_2H_5O + NO_2$		$2.60 \times 10^{-12}\, e^{365/T}$	A
71	$C_2H_5O_2 + NO_2 \xrightarrow{M} C_2H_5O_2NO$	(P) 0.6	$1.20 \times 10^{-29}\, (300/T)^{4.0}$ 9.00×10^{-12}	A
72	$C_2H_5O_2NO_2 \xrightarrow{M} C_2H_5O_2 + NO_2$	(P) 0.31	$4.80 \times 10^{-4}\, e^{-9285/T}$ $8.80 \times 10^{15}\, e^{-10440/T}$	B
73	$C_2H_5O_2 + HO_2 \rightarrow ROOH + O_2$		$7.50 \times 10^{-13}\, e^{700/T}$	A
74	$C_2H_5O + O_2 \rightarrow CH_3CHO + HO_2$		$6.30 \times 10^{-14}\, e^{-550/T}$	A

75	$C_2H_5O + NO \xrightarrow{M} C_2H_5ONO$	(P) 0.6	$2.80\times10^{-27}\ (300/T)^{4.0}$ $5.00\times10^{-12}\ (300/T)^{1.0}$	A
76	$C_2H_5O + NO \rightarrow CH_3CHO + HO_2 + NO$		1.30×10^{-11}	B
77	$C_2H_5O + NO_2 \xrightarrow{M} C_2H_5ONO_2$	(P) 0.6	$2.00\times10^{-27}\ (300/T)^{4.0}$ $2.80\times10^{-11}\ (300/T)^{1.0}$	A
78	$C_3H_8 + OH \rightarrow C_3H_7O_2 + H_2O$		$1.00\times10^{-11}\ e^{-660/T}$	A
79	$C_3H_7O_2 + NO \rightarrow C_3H_7O + NO_2$		$2.70\times10^{-12}\ e^{-660/T}$	B
80	$C_3H_7O + O_2 \rightarrow CH_3COCH_3 + HO_2$		$1.40\times10^{-14}\ e^{-210/T}$	B
81	$C_3H_7O + NO \rightarrow C_3H_7ONO$		3.40×10^{-11}	B
82	$C_3H_7O + NO \rightarrow CH_3COCH_3 + HO_2 + NO$		6.50×10^{-12}	B
83	$C_3H_7O + NO_2 \rightarrow C_3H_7ONO_2$		3.50×10^{-11}	A
84	$C_2H_4 + OH \xrightarrow{M} HOC_2H_4O_2$	(P) 0.6	$1.00\times10^{-28}\ (300/T)^{0.8}$ 8.80×10^{-12}	A
85	$HOC_2H_4O_2 + NO \rightarrow NO_2 + 2\ HCHO + H$		6.93×10^{-12}	A
86	$HOC_2H_4O_2 + NO \rightarrow NO_2 + CH_3CHO + OH$		2.07×10^{-12}	A
87	$C_2H_4 + O_3 \rightarrow HCHO + H_2COO$		$4.48\times10^{-15}\ e^{-2630/T}$	A
88	$C_2H_4 + O_3 \rightarrow HCHO + HCOOH^*$		$7.52\times10^{-15}\ e^{-2630/T}$	A
89	$H_2COO + NO \rightarrow NO_2 + HCHO$		7.00×10^{-12}	C
90	$H_2COO + H_2O \rightarrow HCOOH + H_2O$		4.00×10^{-16}	C
91	$H_2COO + HCHO \rightarrow OZD$		2.00×10^{-12}	C
92	$H_2COO + CH_3CHO \rightarrow OZD$		2.00×10^{-12}	C
93	$H_2COO + ALD2 \rightarrow OZD$		2.00×10^{-12}	C
94	$HCOOH + OH \rightarrow H + CO_2 + H_2O$		4.00×10^{-13}	A
95	$HCOOH^* \rightarrow CO_2 + H_2$		0.21	C
96	$HCOOH^* \rightarrow CO + H_2O$		0.60	C
97	$HCOOH^* \rightarrow OH + HO_2 + CO$		0.19	C
98	$C_3H_6 + OH \xrightarrow{M} HOC_3H_6O_2$	(P) 0.5	$8.00\times10^{-27}\ (300/T)^{3.5}$ 3.00×10^{-11}	B
99	$HOC_3H_6O_2 + NO \rightarrow NO_2 + CH_3CHO + HCHO + HO_2$		6.00×10^{-12}	C
100	$C_3H_6 + O_3 \rightarrow HCHO + CH_3HCOO$		$4.88\times10^{-16}\ e^{-1900/T}$	A
101	$C_3H_6 + O_3 \rightarrow HCHO + CH_3HCOO^*$		$2.76\times10^{-15}\ e^{-1900/T}$	A
102	$C_3H_6 + O_3 \rightarrow CH_3CHO + H_2COO$		$1.22\times10^{-15}\ e^{-1900/T}$	A
103	$C_3H_6 + O_3 \rightarrow CH_3CHO + H_2COO^*$		$2.03\times10^{-15}\ e^{-1900/T}$	A
104	$CH_3HCOO + NO \rightarrow NO_2 + CH_3CHO$		7.00×10^{-12}	C
105	$CH_3HCOO + H_2O \rightarrow CH_3COOH + H_2O$		4.00×10^{-16}	C
106	$CH_3HCOO + HCHO \rightarrow OZD$		2.00×10^{-12}	C
107	$CH_3HCOO + CH_3CHO \rightarrow OZD$		2.00×10^{-12}	C
108	$CH_3HCOO + ALD2 \rightarrow OZD$		2.00×10^{-12}	C
109	$CH_3COOH^* \rightarrow CH_4 + CO_2$		0.16	C
110	$CH_3COOH^* \rightarrow CH_3O_2 + CO + OH$		0.64	C
111	$CH_3COOH^* \rightarrow CH_3O + CO + HO_2$		0.20	C
120	$HCHO + OH \rightarrow HO_2 + CO + H_2O$		$9.00\times10^{-12}\ e^{20/T}$	A
113	$HCHO + O \rightarrow OH + HO_2 + CO$		$3.40\times10^{-11}\ e^{-1600/T}$	A
114	$HCHO + NO_3 \rightarrow HNO_3 + HO_2 + CO$		5.80×10^{-16}	A
115	$HCHO + HO_2 \rightarrow HOCH_2O_2$		$6.70\times10^{-15} e^{605/T}$	A
116	$HOCH_2O_2 \rightarrow HO_2 + HCHO$		$2.40\times10^{12}\ e^{-7000/T}$	B
117	$HOCH_2O_2 + HO_2 \rightarrow ROOH$		$5.60\times10^{-15}\ e^{2300/T}$	B
118	$HOCH_2O_2 + NO \rightarrow NO_2 + HO_2 + HCOOH$		7.00×10^{-12}	C

119	$CH_3CHO + O \rightarrow CH_3C(O)OO + OH$	$1.80\times10^{-11}\ e^{-1100/T}$	A
120	$CH_3CHO + OH \rightarrow CH_3C(O)OO + H_2O$	$5.60\times10^{-12}\ e^{270/T}$	A
121	$CH_3CHO + NO_3 \rightarrow CH_3C(O)OO + HNO_3$	$1.40\times10^{-12}\ e^{-1900/T}$	A
122	$ALD2 + O \rightarrow CH_3C(O)OO + OH$	$1.80\times10^{-11}\ e^{-1100/T}$	A
123	$ALD2 + OH \rightarrow CH_3C(O)OO + H_2O$	$5.60\times10^{-12}\ e^{270/T}$	A
124	$ALD2 + NO_3 \rightarrow CH_3C(O)OO + HNO_3$	$1.40\times10^{-12}\ e^{-1900/T}$	A
125	$CH_3C(O)OO + HO_2 \rightarrow ROOH + O_2$	$4.30\times10^{-13}\ e^{1040/T}$	A
126	$CH_3C(O)OO + HO_2 \rightarrow CH_3O_2 + OH + CO_2$	$3.16\times10^{-13}\ e^{1040/T}$	C
127	$CH_3C(O)OO + NO \rightarrow NO_2 + CH_3O_2 + CO_2$	$8.10\times10^{-11}\ e^{270/T}$	A
128	$CH_3C(O)OO + NO_2 \xrightarrow{M} CH_3C(O)OONO_2$ (P) 0.6	$9.70\times10^{-29}\ (300/T)^{5.6}$ $9.30\times10^{-12}\ (300/T)^{1.5}$	A
129	$CH_3C(O)OONO_2 \xrightarrow{M} CH_3C(O)OO + NO_2$	$k_{123} / (9.0\times10^{-29} \times e^{14000/T})$	A
130	$CH_3C(O)OO + CH_3C(O)OO \rightarrow 2\ CH_3O_2 + O_2$	$2.90\times10^{-12}\ e^{500/T}$	A
131	$CH_3COCH_3 + OH \rightarrow CH_3COCH_2OO + H_2O$	$1.33\times10^{-13} + 3.82\times10^{-11}\ e^{-2000/T}$	A
132	$CH_3COCH_2OO + NO \rightarrow CH_3C(O)OO + HCHO + NO_2$	8.10×10^{-12}	C
133	$CH_3OH + OH \rightarrow HCHO + HO_2 + H_2O$	$6.21\times10^{-12}\ e^{-620/T}$	A
134	$CH_3OH + OH \rightarrow CH_3O + H_2O$	$1.09\times10^{-12}\ e^{-620/T}$	A
135	$C_2H_5OH + OH \rightarrow CH_3CHO + HO_2 + H_2O$	$6.52\times10^{-12}\ e^{-230/T}$	A
136	$C_2H_5OH + OH \rightarrow HOC_2H_4O_2 + H_2O$	$3.80\times10^{-13}\ e^{-230/T}$	A
137	$PAR + OH \rightarrow RO_2 + H_2O$	9.20×10^{-14}	C
138	$PAR + OH \rightarrow RO_2R + H_2O$	7.20×10^{-13}	C
139	$RO_2 + NO \rightarrow NO_2 + HO_2 + CH_3CHO + XOP$	7.70×10^{-12}	C
140	$RO_2 + NO \rightarrow NTR$	$4.40\times10^{-11}\ e^{-1400/T}$	C
141	$RO_2R + NO \rightarrow NO_2 + ROR$	7.00×10^{-12}	C
142	$RO_2R + NO \rightarrow NTR$	$1.20\times10^{-10}\ e^{-1400/T}$	C
143	$ROR + NO_2 \rightarrow NTR$	1.50×10^{-11}	C
144	$NTR \xrightarrow{M} RO_2 + NO_2$	k_{72}	B
145	$ROR \rightarrow KET + HO_2$	1.60×10^{3}	C
146	$ROR \rightarrow KET + DOP$	$2.10\times10^{14}\ e^{-8000/T}$	C
147	$ROR \rightarrow CH_3CHO + DOP + XOP$	$4.00\times10^{14}\ e^{-8000/T}$	C
148	$ROR \rightarrow CH_3COCH_3 + DOP + 2\ XOP$	$4.40\times10^{14}\ e^{-8000/T}$	C
149	$XOP + PAR \rightarrow$	6.80×10^{-12}	C
150	$DOP + PAR \rightarrow RO_2$	5.10×10^{-12}	C
151	$DOP + PAR \rightarrow AO_2 + 2\ XOP$	1.50×10^{-12}	C
152	$DOP + PAR \rightarrow RO_2R$	1.70×10^{-13}	C
153	$DOP + KET \rightarrow CH_3C(O)OO + XOP$	6.80×10^{-12}	C
154	$AO_2 + NO \rightarrow NO_2 + CH_3COCH_3 + HO_2$	8.10×10^{-12}	C
155	$OLE + O \rightarrow 2\ PAR$	$4.10\times10^{-12}\ e^{-324/T}$	C
156	$OLE + O \rightarrow CH_3CHO$	$4.10\times10^{-12}\ e^{-324/T}$	C
157	$OLE + O \rightarrow HO_2 + CO + RO_2$	$1.20\times10^{-12}\ e^{-324/T}$	C
158	$OLE + O \rightarrow RO_2 + XOP + CO + HCHO + OH$	$2.40\times10^{-12}\ e^{-324/T}$	C
159	$OLE + OH \rightarrow CH_3O_2 + CH_3CHO + XOP$	$5.20\times10^{-12}\ e^{504/T}$	C
160	$OLE + O_3 \rightarrow CH_3CHO + H_2COO + XOP$	$2.80\times10^{-15}\ e^{-2105/T}$	C
161	$OLE + O_3 \rightarrow HCHO + CH_3HCOO + XOP$	$2.80\times10^{-15}\ e^{-2105/T}$	C
162	$OLE + O_3 \rightarrow CH_3CHO + HCOOH^* + XOP$	$4.30\times10^{-15}\ e^{-2105/T}$	C
163	$OLE + O_3 \rightarrow HCHO + CH_3COOH^* + XOP$	$4.30\times10^{-15}\ e^{-2105/T}$	C

164	OLE + NO_3 → PNO_2	7.70×10^{-15}	C
165	PNO_2 + NO → DNIT	6.80×10^{-13}	C
166	PNO_2 + NO → HCHO + CH_3CHO + XOP + $2NO_2$	6.80×10^{-12}	C
167	C_4H_6 + OH → CH_3O_2 + CH_3CHO	$1.48\times10^{-11}\ e^{448/T}$	D
168	C_4H_6 + O_3 → 0.5 CH_3CHO + 0.197 H_2COO + XOP + 0.5 HCHO + 0.197 CH_3HCOO + 0.303 H_2COO* + 0.303 CH_3HCOO* + OLE	$2.20\times10^{-14}\ e^{-2431/T}$	E
169	C_4H_6 + NO_3 → PNO_2 + C_2H_4	1.03×10^{-13}	D
	Aromatic Chemistry		
170	C_6H_6 + OH → 0.4 BO_2 + 0.4 H_2O + 0.6 CRES + 0.6 HO_2 + XOP	$3.10\times10^{-12}\ e^{-270/T}$	D
171	TOL + OH → BO_2 + H_2O	$1.70\times10^{-13}\ e^{322/T}$	C
172	TOL + OH → CRES + HO_2	$7.60\times10^{-13}\ e^{322/T}$	C
173	TOL + OH → TO_2	$1.20\times10^{-12}\ e^{322/T}$	C
174	BO_2 + NO → NO_2 + BZA + HO_2	8.10×10^{-12}	C
175	BZA + OH → BZO_2 + H_2O	1.30×10^{-11}	C
176	BZO_2 + NO → NO_2 + PHO_2 + CO_2	2.50×10^{-12}	C
177	BZO_2 + NO_2 → PBZN	8.40×10^{-12}	E
178	PBZN → BZO_2 + NO_2	$1.60\times10^{15}\ e^{-13033/T}$	E
179	PHO_2 + NO → NO_2 + PHO	8.10×10^{-12}	C
180	PHO + NO_2 → NPHN	$1.30\times10^{-11}\ e^{300/T}$	E
181	CRES + OH → CRO + H_2O	1.60×10^{-11}	C
182	CRES + OH → CRO_2 + H_2O	2.50×10^{-11}	C
183	CRES + NO_3 → CRO + HNO_3	2.20×10^{-11}	C
184	CRO + NO_2 → NCRE	1.40×10^{-11}	C
185	CRO_2 + NO → NO_2 + OPEN + HO_2	4.00×10^{-12}	C
186	CRO_2 + NO → NO_2 + ACID + HO_2	4.00×10^{-12}	C
187	TO_2 + NO → NO_2 + OPEN + HO_2	7.30×10^{-12}	C
188	TO_2 + NO → NTR	8.10×10^{-13}	C
189	TO_2 → HO_2 + CRES	4.20	C
190	XYL + OH → CRES + PAR + HO_2	$3.32\times10^{-12}\ e^{116/T}$	C
191	XYL + OH → XLO_2 + H_2O	$1.70\times10^{-12}\ e^{116/T}$	C
192	XYL + OH → TO_2	$5.00\times10^{-12}\ e^{116/T}$	C
193	XYL + OH → XINT	$6.60\times10^{-12}\ e^{116/T}$	C
194	XLO_2 + NO → NO_2 + HO_2 + BZA + PAR	8.10×10^{-12}	C
195	XINT + NO → NO_2 + HO_2 + 2 CH_3COCHO + PAR	8.10×10^{-12}	C
196	CH_3COCHO + OH → MGPX + H_2O	1.50×10^{-11}	B
197	MGPX + NO → NO_2 + $CH_3C(O)OO$ + CO_2	8.10×10^{-12}	C
198	OPEN + OH → OPPX + $CH_3C(O)OO$ + HO_2 + CO	3.00×10^{-11}	C
199	OPEN + O_3 → CH_3CHO + MGPX + HCHO + CO	$1.60\times10^{-18}\ e^{-500/T}$	C
200	OPEN + O_3 → HCHO + CO + OH + 2 HO_2	$4.30\times10^{-18}\ e^{-500/T}$	C
201	OPEN + O_3 → CH_3COCHO	$1.10\times10^{-17}\ e^{-500/T}$	C
202	OPEN + O_3 → $CH_3C(O)OO$ + HCHO + HO_2 + CO	$3.20\times10^{-17}\ e^{-500/T}$	C
203	OPEN + O_3 →	$5.40\times10^{-18}\ e^{-500/T}$	C
204	OPPX + NO → NO_2 + HCHO + HO_2 + CO	8.10×10^{-12}	C
	Terpene Chemistry		
200	ISOP + OH → ISOH	$2.55\times10^{-11}\ e^{410.2/T}$	F,G
201	ISOP + O_3 → 0.17 MACR + 0.378 MVK + 0.664 OH+ 0.054PAR + 0.054 OLE + 0.054 H_2COO + 0.5 HCHO + 0.366 HO_2 + 0.068 CO_2 + 0.461 CO+ 0.366RO2R + 0.121	$7.86\times10^{-15}\ e^{-1912.9/T}$	G,H

	ACID		
202	ISOP + O → 0.22 MACR + 0.63 MVK + 0.08 ISOH	3.50×10^{-11}	F,G
203	ISOP + NO_3 → ISNT	$3.02\times10^{-12}\ e^{-445.9/T}$	F,G
204	ISOH + NO → 0.364 MACR + 0.477 MVK + 0.840 HCHO + 0.08 ISNI1 + 0.08 ISNI2 + 0.886 HO_2 + 0.840 NO_2	$1.22\times10^{-11}\ e^{-180/T}$	F
205	ISNT + NO → 1.1 NO_2 + 0.8 HO_2 + 0.80 ISNI1 + 0.1 MACR + 0.15 HCHO + 0.05 MVK + 0.05 DISN	$1.39\times10^{-11}\ e^{-180/T}$	F
206	ISNI1 + OH → ISNIR	3.35×10^{-11}	F
207	ISNI2 + OH → ISNIR	1.88×10^{-11}	F
208	ISNIR + NO → 0.05 DISN + 0.05 HO_2 + 1.9 NO_2 + 0.95 CH_3CHO + 0.95 CH_3COCH_3	$1.39\times10^{-11}\ e^{-180/T}$	F
209	ISNI1 + O_3 → 0.2 O + 0.08 OH + 0.5 HCHO + 0.5 IALD1 + 0.5 ISNI2 + 0.5 NO_2	5.00×10^{-18}	F
210	ISOH + ISOH → 0.6 MACR + 0.6 MVK + 1.2 HCHO + 1.2 HO_2	2.00×10^{-13}	F
211	ISOH + HO_2 → IPRX	$6.15\times10^{-11}\ e^{-900/T}$	F
212	IPRX + OH → ISOH	2.00×10^{-11}	F
213	IPRX + O_3 → 0.7 HCHO	8.00×10^{-18}	F
214	MACR + O_3 → 0.8 CH_3COCHO + 0.7 HCHO + 0.2 O + 0.09 H_2COO + 0.2 CO + 0.275 HO_2 + 0.215 OH + 0.16 CO_2 + 0.15 CH_2CCH_3CHOO	$1.36\times10^{-15}\ e^{-2113.7/T}$	F,H
215	MVK + O_3 - → 0.5 CH_3COCHO + 0.5 HCHO + 0.2 H_2O + 0.2 CO_2 + 0.56 CO + 0.28 HO_2 + 0.36 OH + 0.1 CH_3CHO + 0.28 CH_3CO_3 + 0.12 ACID + 0.12 UNR	$7.50\times10^{-16}\ e^{-1519.9/T}$	H
216	MACR + OH → 0.42 MAC1 + 0.08 MAC2 + 0.5 $CH_2CCH_3C(O)OO$	$1.86\times10^{-11}\ e^{175/T}$	F
217	MVK + OH → 0.28 MV1 + 0.72 MV2	$4.11\times10^{-12}\ e^{453/T}$	F
218	MAC1 + NO → 0.95 HO_2 + 0.95 CO + 0.95 CH_3COCH_3 + 0.95 NO_2 + 0.05 ISNI2	$1.39\times10^{-11}\ e^{-180/T}$	F
219	MAC2 + NO → 0.95 HO_2 + 0.95 HCHO + 0.95 CH_3COCHO + 0.95 NO_2 + 0.05 ISNI2	$1.39\times10^{-11}\ e^{-180/T}$	F
220	MV1 + NO → 0.95 CH_3COCHO + 0.95 HCHO + 0.05 ISNI2 + 0.95 NO_2 + 0.95 HO_2	$1.39\times10^{-11}\ e^{-180/T}$	F
221	MV2 + NO → 0.95 CH_3CHO + 0.95 $CH_3C(O)OO$ + 0.05 ISNI2 + 0.95 NO_2	$1.39\times10^{-11}\ e^{-180/T}$	F
222	MV1 + HO_2 → ROOH	$6.15\times10^{-11}\ e^{-900/T}$	F
223	MV2 + HO_2 → ROOH	$6.15\times10^{-11}\ e^{-900/T}$	F
224	MAC1 + HO_2 → ROOH	$6.15\times10^{-11}\ e^{-900/T}$	F
225	MAC2 + HO_2 → ROOH	$6.15\times10^{-11}\ e^{-900/T}$	F
226	$CH_2CCH_3C(O)OO$ + NO_2 → MPAN	8.40×10^{-12}	F
227	MPAN → $CH_2CCH_3C(O)OO$ + NO_2	$1.58\times10^{16}\ e^{-13507/T}$	F
228	$CH_2CCH_3C(O)OO$ + NO → C_2H_4 + CH_3O_2 + NO_2 + CO_2	1.40×10^{-11}	F
229	TERPH + OH → RO227	1.77×10^{-10}	H
230	TERPH + O_3 → 0.445 CO + 0.055 H_2O_2 + 0.89 OH + 0.11 UNR + 0.445 RO229 + 0.445 RO230	1.40×10^{-16}	H
231	TERPH + O → UNR	8.59×10^{-11}	H
232	TERPH + NO_3 → RO228	2.91×10^{-11}	H
233	RO227 + NO → 0.38 AP8 + 0.62 NO_2 + 0.62 HO_2 + 0.62 UNR	$8.89\times10^{-13}\ e^{180.2/T}$	H

234	RO227+ RO2R $\rightarrow$ HO_2 + UNR + RO2R + O_2		1.00×10^{-15}	H
235	RO227 + HO_2 $\rightarrow$ OH + HO_2 + UNR		$3.41\times10^{-13}\ e^{800.2/T}$	H
236	RO228 + NO $\rightarrow$ 2 NO_2 + UNR		$8.89\times10^{-13}\ e^{180.2/T}$	H
237	RO228 + RO2R $\rightarrow$ NO_2 + RO2R + O_2 + UNR		1.00×10^{-15}	H
238	RO229 + HO_2 $\rightarrow$ OH + HO_2 + UNR		$3.41\times10^{-13}\ e^{800.2/T}$	H
239	RO229 + NO $\rightarrow$ 0.23 AP9 + 0.77 NO_2 + 0.77 RO240		$1.05\times10^{-12}\ e^{180.2/T}$	H
240	RO229 + RO2R $\rightarrow$ RO240 + RO2R + O_2		1.00×10^{-15}	H
241	RO230 + NO $\rightarrow$ NO_2 + CH_3CO_3 + UNR		$8.89\times10^{-13}\ e^{180.2/T}$	H
242	RO230 + RO2R $\rightarrow$ CH_3CO_3 + RO2R + O_2 + UNR		1.00×10^{-15}	H
243	RO230 + HO_2 $\rightarrow$ OH + CH_3CO_3 + UNR		$3.41\times10^{-13}\ e^{800.2/T}$	H
244	RO240 + NO $\rightarrow$ NO_2 + CH_3CO_3 + ALD2 + PAR		$1.05\times10^{-12}\ e^{180.2/T}$	H
245	RO240 + RO2R $\rightarrow$ CH_3CO_3 + ALD2 + PAR + RO2R + O_2		1.00×10^{-15}	H
246	RO240 + HO_2 $\rightarrow$ OH + CH_3CO_3 + ALD2 + PAR		$3.41\times10^{-13}\ e^{800.2/T}$	H
247	AP8 + OH $\rightarrow$ NO_2 + H_2O + UNR		1.03×10^{-10}	H
248	AP9 + OH $\rightarrow$ NO_2 + H_2O + UNR		9.07×10^{-11}	H
	Sulfur Chemistry			
249	SO_2 + OH $\xrightarrow{M}$ HSO_3	(P) 0.6	$3.00\times10^{-31}\ (300/T)^{3.3}$ 1.50×10^{-12}	A
250	SO_2 + O + M $\rightarrow$ SO_3 + M		$1.30\times10^{-33}\ (300/T)^{-3.6}$	A
251	HSO_3 + O_2 $\rightarrow$ SO_3 + HO_2		$1.30\times10^{-12}\ e^{-330/T}$	A
252	SO_3 + H_2O + H_2O $\rightarrow$ H_2SO_4 + H_2O		$8.50\times10^{-41}\ e^{6540/T}$	A
253	CH_3SCH_3 + OH $\rightarrow$ $CH_3SCH_2O_2$ + H_2O		$1.10\times10^{-11}\ e^{-240/T}$	A
254	CH_3SCH_3 + OH $\rightarrow$ $CH_3S(OH)CH_3$		f	A
255	$CH_3SCH_2O_2$ + NO $\rightarrow$ CH_3SCH_2O + NO_2		8.00×10^{-12}	I
256	CH_3SCH_2O $\rightarrow$ CH_3S + HCHO		1.00×10^{1}	I
257	CH_3S + O_2 $\rightarrow$ CH_3SOO*		3.00×10^{-18}	A
258	CH_3SOO* + NO $\rightarrow$ CH_3SO + NO_2		1.4×10^{-11}	I
259	CH_3SOO* $\rightarrow$ CH_3S + O_2		6.0×10^{2}	I
260	CH_3SO + O_3 $\rightarrow$ CH_3SO_2 + O_2		6.0×10^{-13}	A
261	CH_3SO_2 $\rightarrow$ CH_3O_2 + SO_2		1.1×10^{1}	I
262	$CH_3S(OH)CH_3$ $\rightarrow$ CH_3SOH + CH_3O_2		5.0×10^{5}	I
263	CH_3SOH + OH $\rightarrow$ CH_3SO + H_2O		1.1×10^{-10}	I
	Chlorine Gas-Phase Chemistry			
264	Cl + O_2 $\xrightarrow{M}$ ClOO	(P) 0.6	$2.20\times10^{-33}\ (300/T)^{3.1}$ 1.80×10^{-10}	A
265	ClOO + M $\rightarrow$ Cl + O_2 + M		K_{264} / ($6.60\times10^{-25}\times e^{2502/T}$)	A
266	Cl + O_3 $\rightarrow$ ClO + O_2		$2.30\times10^{-11}\ e^{-200/T}$	A
267	Cl + H_2 $\rightarrow$ HCl + H		$3.05\times10^{-11}\ e^{-2270/T}$	A
268	Cl + HO_2 $\rightarrow$ HCl + O_2		$1.80\times10^{-11}\ e^{170/T}$	A
269	Cl + HO_2 $\rightarrow$ ClO + OH		$4.10\times10^{-11}\ e^{-450/T}$	A
270	Cl + H_2O_2 $\rightarrow$ HCl + HO_2		$1.10\times10^{-11}\ e^{-980/T}$	A
271	Cl + NO_2 $\xrightarrow{M}$ $ClNO_2$	(P) 0.6	$1.80\times10^{-31}\ (300/T)^{2.0}$ $1.00\times10^{-10}(300/T)^{1.0}$	A
272	Cl + HNO_3 $\rightarrow$ HCl + NO_3		2.00×10^{-16}	A
273	Cl + CH_4 $\rightarrow$ HCl + CH_3O_2		$7.30\times10^{-12}\ e^{-1280/T}$	A
274	Cl + HOCl $\rightarrow$ Cl_2 + OH		$2.50\times10^{-12}\ e^{-130/T}$	A
275	Cl + OClO $\rightarrow$ ClO + ClO		$3.40\times10^{-12}\ e^{160/T}$	A
276	Cl + ClOO $\rightarrow$ Cl_2 + O_2		2.30×10^{-10}	A

277	$ClO + O \rightarrow Cl + O_2$		$2.80\times10^{-11}\ e^{85/T}$	A
278	$ClO + O_3 \rightarrow ClOO + O_2$		1.40×10^{-17}	A
279	$ClO + OH \rightarrow Cl + HO_2$		$7.40\times10^{-12}\ e^{270/T}$	A
280	$ClO + OH \rightarrow HCl + O_2$		$6.00\times10^{-13}\ e^{230/T}$	A
281	$ClO + HO_2 \rightarrow HOCl + O_2$		$2.70\times10^{-12}\ e^{220/T}$	A
282	$ClO + NO \rightarrow Cl + NO_2$		$6.40\times10^{-12}\ e^{290/T}$	A
283	$ClO + NO_2 \xrightarrow{M} ClONO_2$	(P) 0.6	$1.80\times10^{-31}\ (300/T)^{3.4}$ $1.50\times10^{-11}(300/T)^{1.9}$	A
284	$ClO + ClO \rightarrow Cl + ClOO$		$3.00\times10^{-11}\ e^{-2450/T}$	A
285	$ClO + ClO \xrightarrow{M} Cl_2O_2$	(P) 0.6	$1.60\times10^{-32}\ (300/T)^{4.5}$ $2.00\times10^{-12}(300/T)^{2.4}$	A
286	$Cl_2O_2 + M \rightarrow ClO + ClO + M$		$K_{285}\ /\ (9.30\times10^{-28} \times e^{8835/T})$	A
287	$HCl + OH \rightarrow Cl + H_2O$		$2.60\times10^{-12}\ e^{-350/T}$	A
288	$ClONO_2 + O \rightarrow Cl + NO_2 + O_2$		$2.90\times10^{-12}\ e^{-800/T}$	A
289	$ClNO_2 + OH \rightarrow HOCl + NO_2$		$2.40\times10^{-12}\ e^{-1250/T}$	A
290	$OClO + O \rightarrow ClO + O_2$		$2.40\times10^{-12}\ e^{-960/T}$	A
291	$OClO + OH \rightarrow HOCl + O_2$		$4.50\times10^{-13}\ e^{800/T}$	A
292	$OClO + NO \rightarrow ClO + NO_2$		$2.50\times10^{-12}\ e^{-600/T}$	A
293	$HOCl + O \rightarrow ClO + OH$		1.70×10^{-13}	A
294	$HOCl + OH \rightarrow ClO + H_2O$		$3.00\times10^{-12}\ e^{-500/T}$	A
295	$Cl_2 + OH \rightarrow HOCl + Cl$		$1.40\times10^{-12}\ e^{-900/T}$	A
296	$CH_3Cl + OH \rightarrow HCHO + ClO + H_2O$		$2.40\times10^{-12}\ e^{-1250/T}$	A
	Bromine Gas-Phase Chemistry			
297	$Br + O_3 \rightarrow BrO + O_2$		$1.70\times10^{-11}\ e^{-800/T}$	A
298	$Br + HO_2 \rightarrow HBr + O_2$		$4.80\times10^{-12}\ e^{-310/T}$	A
299	$Br + H_2O_2 \rightarrow HBr + HO_2$		$1.00\times10^{-11}\ e^{-3000/T}$	A
300	$Br + HCHO \rightarrow HBr + CO + HO_2$		$1.70\times10^{-11}\ e^{-800/T}$	A
301	$BrO + O \rightarrow Br + O_2$		$1.90\times10^{-11}\ e^{230/T}$	A
302	$BrO + OH \rightarrow Br + HO_2$		$1.70\times10^{-11}\ e^{250/T}$	A
303	$BrO + HO_2 \rightarrow HOBr + O_2$		$4.50\times10^{-12}\ e^{460/T}$	A
304	$BrO + NO \rightarrow Br + NO_2$		$8.80\times10^{-12}\ e^{260/T}$	A
305	$BrO + NO_2 \xrightarrow{M} BrONO_2$	(P) 0.6	$5.20\times10^{-31}\ (300/T)^{3.2}$ $6.90\times10^{-12}(300/T)^{2.9}$	A
306	$BrO + ClO \rightarrow Br + OClO$		$9.50\times10^{-13}\ e^{550/T}$	A
307	$BrO + ClO \rightarrow Br + Cl + O_2$		$2.30\times10^{-13}\ e^{260/T}$	A
308	$BrO + ClO \rightarrow BrCl + O_2$		$4.10\times10^{-13}\ e^{290/T}$	A
309	$BrO + BrO \rightarrow 2Br + O_2$		$2.40\times10^{-12}\ e^{40/T}$	A
310	$BrO + BrO \rightarrow Br_2 + O_2$		$2.80\times10^{-14}\ e^{860/T}$	A
311	$BrO + O_3 \rightarrow Br + 2O_2$		$1.00\times10^{-12}\ e^{-3200/T}$	A
312	$HBr + OH \rightarrow Br + H_2O$		$5.50\times10^{-12}\ e^{200/T}$	A
313	$HOBr + O \rightarrow BrO + OH$		$1.20\times10^{-10}\ e^{-430/T}$	A
314	$BrCl + O \rightarrow BrO + Cl$		2.20×10^{-11}	A
	Heterogeneous Chemistry			
315	$N_2O_5 + H_2O(a) \rightarrow 2\ HNO_3(a)$		Aer. (J,A), ice (L), NAT (L), liq. (A)	
316	$N_2O_5 + HCl(a) \rightarrow ClNO_2 + HNO_3(a)$		Aer. (A), ice (L), NAT (L)	
317	$ClONO_2 + H_2O \rightarrow HOCl + HNO_3(a)$		Aer. (K), ice (L), NAT (L), liq. (A)	
318	$ClONO_2 + HCl(a) \rightarrow Cl_2 + HNO_3(a)$		Aer. (K), ice (L), NAT (L)	
319	$HOCl + HCl(a) \rightarrow Cl_2 + H_2O(s)$		Aer. (K), ice (L), NAT (L)	
320	$BrONO_2 + H_2O \rightarrow HOBr + HNO_3(a)$		Aer. (A), ice (A), liq. (A)	

321	$BrONO_2 + HCl(a) \rightarrow BrCl + HNO_3(a)$	Aer. (A), ice (A)	
322	$HOBr + HCl(a) \rightarrow BrCl + H_2O(s)$	Aer. (A), ice (A)	
323	$HOBr + HBr(a) \rightarrow Br_2 + H_2O(a)$	Aer. (A), ice (A)	
	Photoprocesses		
324	$O_2 + h\nu \rightarrow O + O$		A
325	$O_3 + h\nu \rightarrow O(^1D) + O_2$		A
325	$O_3 + h\nu \rightarrow O + O_2$		A
327	$HO_2 + h\nu \rightarrow OH + O(^1D)$		A
328	$H_2O + h\nu \rightarrow H + OH$		A
329	$H_2O_2 + h\nu \rightarrow 2\ OH$		A
330	$NO_2 + h\nu \rightarrow NO + O$		A
331	$NO_3 + h\nu \rightarrow NO_2 + O$		B
332	$NO_3 + h\nu \rightarrow NO + O_2$		B
333	$N_2O + h\nu \rightarrow N_2 + O(1D)$		A
334	$N_2O_5 + h\nu \rightarrow NO_2 + NO_3$		A
335	$HONO + h\nu \rightarrow OH + NO$		A
336	$HONO + h\nu \rightarrow H + NO_2$		A
337	$HNO_3 + h\nu \rightarrow OH + NO_2$		A
338	$HNO_3 + h\nu \rightarrow HONO + O(^1D)$		A
339	$HNO_3 + h\nu \rightarrow OH + NO + O$		A
340	$HO_2NO_2 + h\nu \rightarrow HO_2 + NO_2$		B
341	$HO_2NO_2 + h\nu \rightarrow OH + NO_3$		B
342	$HCHO + h\nu \rightarrow 2\ HO_2 + CO$		A
343	$HCHO + h\nu \rightarrow CO + H_2$		A
344	$CH_3OOH + h\nu \rightarrow CH_3O + OH$		B
345	$CH_3CHO + h\nu \rightarrow CH_3O_2 + HO_2 + CO$		B
346	$ALD2 + h\nu \rightarrow CH_3O_2 + HO_2 + CO$		B
347	$CH_3ONO + h\nu \rightarrow CH_3O + NO$		C
348	$CH_3ONO_2 + h\nu \rightarrow CH_3O + NO_2$		B
349	$CH_3O_2NO_2 + h\nu \rightarrow CH_3O_2 + NO_2$		B
350	$C_2H_5ONO_2 + h\nu \rightarrow C_2H_5O + NO_2$		B
351	$C_3H_7ONO_2 + h\nu \rightarrow C_3H_7O + NO_2$		B
352	$CH_3CO_3NO_2 + h\nu \rightarrow CH_3CO_3 + NO_2$		A
353	$CH_3COCH_3 + h\nu \rightarrow CH_3O_2 + CH_3C(O)OO$		B
354	$KET + h\nu \rightarrow CH_3C(O)OO + RO_2 + 2XOP$		J
355	$MVK + h\nu \rightarrow CH_3C(O)OO + C_2H_4 + HO_2$		K
356	$MACR + h\nu \rightarrow C_2H_4 + HO_2 + CO + CH_3O_2$		A
357	$CH_3COCHO + h\nu \rightarrow CH_3C(O)OO+CO+HO_2$		B
358	$BZA + h\nu \rightarrow PHO_2 + CO + HO_2$		C
359	$OPEN + h\nu \rightarrow CH_3C(O)OO + CO + HO_2$		C
360	$HCl + h\nu \rightarrow H + Cl$		A
361	$ClO + h\nu \rightarrow Cl + O$		A
362	$ClOO + h\nu \rightarrow ClO + O$		A
363	$OClO + h\nu \rightarrow ClO + O$		A
364	$HOCl + h\nu \rightarrow OH + Cl$		A
365	$ClONO_2 + h\nu \rightarrow Cl + NO_3$		A
366	$ClONO_2 + h\nu \rightarrow ClO + NO_2$		A
367	$Cl_2 + h\nu \rightarrow Cl + Cl$		A
368	$Cl_2O_2 + h\nu \rightarrow Cl + ClOO$		A
369	$ClNO_2 + h\nu \rightarrow Cl + NO_2$		A
370	$CH_3Cl + h\nu \rightarrow HCHO + ClO + HO_2$		A
371	$CFCl_3 + h\nu \rightarrow 3Cl + F + CO_2$		A
372	$CF_2Cl_2 + h\nu \rightarrow 2\ Cl + 2F + CO_2$		A
373	$BrO + h\nu \rightarrow Br + O$		A
374	$HOBr + h\nu \rightarrow Br + OH$		A

374	$BrONO_2 + h\nu \rightarrow Br + NO_3$		A
376	$BrONO_2 + h\nu \rightarrow BrO + NO_2$		A
377	$Br_2 + h\nu \rightarrow Br + Br$		A
378	$CH_3Br + h\nu \rightarrow CH_3O_2 + Br$		A
379	$HBr + h\nu \rightarrow H + Br$		A
380	$BrCl + h\nu \rightarrow Br + Cl$		A

Species names are defined in Appendix Table B.3. of *Jacobson* [2005b]. In addition, C_4H_6=1,3-butadiene, C_6H_6=benzene., ALD2=C_3 and higher aldehydes, TERPH = monoterpenes. Species above reaction arrows are second or third bodies included in pressure-dependent reactions (footnote *a*) or in thermal dissociation reactions in equilibrium with the forward (previous) reaction. M is total air. The "Ref." column refers to sources of data for reaction rate coefficients, absorption cross sections, and quantum yields.

a (P) indicates a pressure-dependent reaction, for which the reaction rate coefficient is

$$k_r = \frac{k_{\infty,T} k_{0,T}[\mathrm{M}]}{k_{\infty,T} + k_{0,T}[\mathrm{M}]} F_c^{\left[1 + \left(\log_{10} \frac{k_{0,T}[\mathrm{M}]}{k_{\infty,T}}\right)^2\right]^{-1}}$$

where $k_{0,T}$ is the temperature-dependent three-body, low-pressure limit rate coefficient (the first rate listed), $k_{\infty,T}$ is the two-body, high-pressure limit rate coefficient (the second rate listed), [M] = $[N_2]$ + $[O_2]$ is the concentration (molecules cm^{-3}) of the third body, and F_c is the broadening factor.

b A, [*Sander et al*., 2006]; B, *Atkinson et al*. [1997]; C, *Gery et al*. [1988; 1989]; D, MCM Mechanism (http://mcm.leeds.ac.uk/MCM); E, *Bahta et al*. [2004] (assume products the same as OLE+O_3 plus OLE; F, *Paulson and Seinfeld* [1992]; G, *Atkinson* [1997]; H, *Griffin et al*. [2002]; G, *Yin et al*. [1990]; H, assumed the same as for acetone; I, assumed the same as for methyl ethyl ketone; J, *Robinson et al*., 1997; K, *Shi et al*. 2001; L, *Tabazadeh and Turco*, 1993.

c $k_r = k_1 + k_3[\mathrm{M}] / (1 + k_3[\mathrm{M}]/k_2)$, where $k_1 = 2.40\times10^{-14}\ e^{460/T}$, $k_2 = 2.70\times10^{-17}\ e^{2199/T}$, $k_3 = 6.50\times10^{-34}\ e^{1335/T}$, and [M] = $[N_2]$ + $[O_2]$ (molecules cm^{-3}).

d $k_r = 1.50\text{x}10^{-13}(1+0.6\ p_a)(300/T)^{1.0}$, where p_a is the ambient air pressure in atmospheres.

e $k_r = (2.30\times10^{-13}\ e^{600/T} + 1.70\times10^{-33}[\mathrm{M}]e^{1000/T})(1. + 1.40\times10^{-21}[H_2O]e^{2200/T})$, where [M] = $[N_2]$ + $[O_2]$ and $[H_2O]$ are in units of molecules cm^{-3}.

f $k_r = 1.0\text{x}10^{-39}[\mathrm{M}]e^{5820/T}/(1+5.0\text{x}10^{-30}[\mathrm{M}]e^{6280/T})$, where [M] = $[N_2]$ + $[O_2]$ (molecules cm^{-3}) .

1
2